



Evaluation of CMIP6 models for simulations of surplus/deficit summer monsoon conditions over India

Gopinadh Konda¹ · Naresh Krishna Vissa¹

Received: 28 January 2022 / Accepted: 26 May 2022 / Published online: 17 June 2022
© The Author(s), under exclusive licence to Springer-Verlag GmbH Germany, part of Springer Nature 2022

Abstract

This study uses the 30 General Circulation Models (GCMs) from the Coupled Model Intercomparison Project phase-6 (CMIP6) to examine the simulations of the surplus/deficit Indian summer monsoon rainfall (ISMR) and its associated air-sea interactions on intraseasonal to interannual timescales. The majority of the CMIP6 models simulate the seasonal mean state of ISMR over the Indian mainland with systematic biases. Best performing models (BPM; AWI-ESM-1-1-LR, BCC-CSM2-MR, BCC-ESM1, CNRM-CM6-1, CNRM-ESM2-1, GFDL-CM4, INM-CM5-0, MIROC-ES2L, MIROC6, TaiESM1) well simulated the seasonal mean precipitation with Taylor skill score > 0.75 and normalized root mean square error (NRMSE) is < 0.7 . However, the models are failed to simulate precipitation over the orographic regions (Western Ghats). Improving the simulations of low-level winds and sea surface temperature (SST) with high spatial resolutions would provide better precipitation simulations. B-MME (multimodel ensemble mean of BPM) can capture the negative IOD-like (Indian Ocean Dipole) pattern during deficit monsoon years and fail to capture the positive IOD-like pattern during surplus monsoon years. Models overestimate the moisture transport from the West Indian Ocean to the sub-continent of India during deficit monsoons, which plays a crucial role in modulating the precipitation and its associated intraseasonal variability. The present analysis identified that during deficit monsoon years, the faster moving 20–100 days oscillations are evident; however, these oscillations are sluggish during surplus monsoon years, which affects the duration of convection activity and causes dry conditions over the regions. During surplus monsoon years, the Bay of Bengal (Arabian Sea) responds strongly (slowly) to the atmosphere than the deficit monsoon years. However, models are fail to represent the ocean's response to the atmosphere over the Bay of Bengal. The freshwater forcing improvement in the models simulates the ocean to atmosphere response over the Indian region. The present study further suggests that the improved simulation of the Indian summer monsoon (ISM) variability by the GCMs is possible by improving the ocean and atmosphere feedback mechanisms, sensitivities of the models among internal variables, and orographic features necessary for the accurate simulation of intraseasonal variability.

Keywords Indian summer monsoon · Flood (surplus)/drought (deficit) · CMIP6 models · Intraseasonal oscillations · Air-sea interactions

1 Introduction

The Asian monsoon system (AMS) is a largescale phenomenon resulting in the strong coupling of the ocean and atmosphere, and is highly associated with remote forcings. The present study focuses on the Indian summer monsoon (ISM) system. ISM covers a large area and persists from

June to September (JJAS), and about 80% of the annual rainfall occurs over the Indian mainland during this season (Gadgil 2003). The ISM rainfall (ISMR) is highly variable from intraseasonal through interannual to decadal timescales (Goswami et al. 1999; Gadgil and Gadgil 2006; Turner and Annamalai 2012; Goswami et al. 2015; Preethi et al. 2017a, b; Srivastava et al. 2017). Many studies have analysed the impact of El Niño Southern Oscillation (ENSO; Rasmusson and Wallace 1983) on ISMR (Kriplani and Kulkarni 1997; Goswami 1998; Wang and Li 2004; Wang 2006; Mishra et al. 2012; Shin et al. 2019; Ashok et al. 2019; Seetha et al. 2020). ENSO is the dominant mode of interannual variability of the tropical Pacific Ocean that affects the

✉ Naresh Krishna Vissa
vissan@nitrkl.ac.in; vissanaresh@gmail.com

¹ Department of Earth and Atmospheric Sciences, National Institute of Technology Rourkela, Dist: Sundargarh, Rourkela, Odisha 769008, India

ISMR (Kripalani and Kulkarni 1997; Kumar et al. 1999; Krishnamurthy and Goswami 2000; Ashok et al. 2001; Annamalai et al. 2007; Bracco et al. 2007; Kucharski and Abid 2017; Yun and Timmermann 2018; Pandey et al. 2020; Hrudya et al. 2021; Yang and Huang 2021). In addition, Indian Ocean Dipole (IOD; Saji et al. 1999; Ashok et al. 2004) is another dominant phenomenon that occurs in the tropical Indian Ocean and significantly affects the ISMR (Ashok et al. 2001; Krishnan et al. 2011; Chowdary et al. 2016; Srivastava et al. 2019). Krishnaswamy et al. (2015) suggested that ENSO and IOD are the significant drivers of the ISMR. Many studies reported the combined and individual influence of ENSO and IOD on ISMR (Ashok et al. 2004; Sikka and Ratna 2011; Krishnaswamy et al. 2015; Hrudya et al. 2020). Ashok et al. (2007) identified the El Niño Modoki, a coupled ocean–atmosphere phenomenon that occurs over the tropical central Pacific. Typical El Niño Modoki and La Niña Modoki affect the ISMR (Dandi et al. 2020) by inducing changes in the western Pacific low-level circulation. Recent studies identified the strong relationship between ISMR and equatorial Indian Ocean Oscillations (EQUINOO) (Gadgil et al. 2004; Surendran et al. 2015). In addition, the Atlantic Niño (Yadav et al. 2018a, b), western North Pacific circulation variations (Chowdary et al. 2019), tropical Indian Ocean basin-wide warming (Chowdary et al. 2015; Chakravorty et al. 2016) also play an important role in modulating the monsoon interannual and decadal variability (Yadav 2017). This interannual phenomenon directly/indirectly affects the ISMR and causes surplus and deficit monsoon rainfall over the regions of India (Wang 2006).

The seasonal prediction of ISMR highly depends on the interannual variability (Pillai and Chowdary 2016), although the interannual variability of ISMR is highly modulated by the intraseasonal oscillations (ISO) (Krishnamurthy and Shukla 2007; Krishnamurthy and Sharma 2017). ISM's active and break spells are manifestations of ISO (Goswami 2005, Goswami et al. 2006; Rajeevan et al. 2006; 2010; Suhas et al. 2013) of the northward shift intertropical convergence zone (ITCZ; Sikka 1980). Krishnan et al. (2006) suggested that the intraseasonal evolution of the ocean–monsoon coupled system plays a vital role in unlocking the dynamics of monsoon droughts. Many recent studies identified the important role of ISO during the excess monsoon years (Kumar et al. 2010; Preethi et al. 2017a, b; Shrivastava and Kar 2017). The convection anomalies develop in the equatorial Indian Ocean and propagate northward on 20–100 days, known as boreal summer ISO (BSISO) (Kikuchi et al. 2012), and are closely associated with the active and break spells of the ISMR (Lawrence and Webster 2002). BSISO can support intense monsoonal precipitation (Webster et al. 1998; Mao and Chan 2005), monsoon depressions (Krishnamurthy and Ajayamohan 2010; Karmakar et al. 2021), and the manifestation of extreme events (Li et al. 2016; Hsu et al. 2017;

Sun et al. 2018). However, northward moving convection shows a considerable disparity in the periodicity within the same season (Lawrence and Webster 2001, 2002), and certain summers exhibit prominent northward propagation of convection, whereas, in other summers, the northward propagations are irregular (Singh and Kripalani 1985). Several studies suggest that ISO act as the source for the interannual variability of the monsoon, further supporting the ISM's strength (Goswami and Mohan 2001; Suhas et al. 2011). Kulkarni et al. (2009) studied the intraseasonal variability during excess/deficit monsoon years. They identified that the faster moving high frequency (10–20 days) oscillations during excess monsoons are stronger than the slow-moving low frequency (30–60 days) oscillations. Madden–Julian Oscillations (MJO; Madden and Julian 1971, 1972) is another mode of intraseasonal variability in the tropics and is prominent in the equatorial region during boreal winter (Dec to Feb). MJO is characterized by largescale convection anomalies developing over the west equatorial Indian Ocean and propagating eastward on a timescale of 30–50 days (Joseph et al. 2010). MJO is relatively weaker and has a complex structure in the boreal summer (Kikuchi et al. 2012; Lee et al. 2013), can influence the climate and weather systems in the tropics, and extend to extratropics (Li and Lu 2020). Saith and Slingo (2006) suggested that westerly wind burst in the western Pacific is associated with the MJO, leads to the extension of warm sea surface temperature (SST) anomalies to the east, initiating the El Niño, creating a long break over the Indian region and a monsoon drought. Joseph et al. (2009) identified that the propensity of eastward propagating MJO during boreal summer is largely responsible for the monsoon droughts. Anandh and Vissa (2020) suggested that eastward propagating MJO over the Indian Ocean can modulate the rainfall over the Indian mainland, and the MJO influences more than 50% of weather phenomena on different timescales (Roxy et al. 2019).

Recent studies used the coupled General Circulation Models (GCMs) to forecast the ISMR (Kulkarni et al. 2012; Saha et al. 2019). National Centers for Environmental Prediction (NCEP) Coupled Forecast System version-2 (CFSv2; Saha et al. 2014) is used to examine the forecast of ISMR its associated teleconnections (Shukla 2014; Shukla and Huang 2016; Shin et al. 2019; Shukla and Shin 2020). Recently, Dutta et al. (2020) used the CFSv2 model to examine the active-break spells of the ISMR; they suggested that the ice-phase microphysics parameterization scheme well captures the active-break spells than the ice-free parameterization scheme. The accurate representation of the exchange of air–sea fluxes at the air–sea interface is necessary to predict the monsoonal precipitation by the coupled models (Fu et al. 2002; Wang 2005; Ratnam et al. 2009; Konda and Vissa 2021). GCMs, which several modeling groups develop across the world under the CMIP phase-6 (CMIP6), were extensively used to study the impacts

of climate changes across the globe during different epochs (Eyring et al. 2016). Almazroui et al. (2020, 2021) analyzed the CMIP6 future projections, they identified that the increase of annual mean precipitation in the future scenario over South Asia during the twenty-first century and the rate of change in the projected annual mean precipitation varies considerably between the South Asian countries (Dai et al. 2022). Recent studies suggest that CMIP6 models simulate the ISMR better than the CMIP5 models (Xin et al. 2020; Gusain et al. 2020; Rajendran et al. 2021). Compared to the CMIP5 models, the new release of CMIP6 models shows a significant increase of skill in representing the MJO propagation (Ahn et al. 2020). Rajendran et al. (2021) analysed the multimodel ensemble mean (MME) of CMIP6 and AMIP6 models in simulating the interannual variability and its teleconnections with rainfall variability over the equatorial Pacific and Indian Oceans. They found that CMIP6 models show the best skill in simulating the monsoon rainfall over India compared to the AMIP6 models. The CMIP6 provided an opportunity to examine models' ability to simulate the characteristic features of ISO and analyse the air-sea interactions on intraseasonal timescales. Recently, Jain et al. (2021) identified the shifting of Somali Jet (Jet) over India during flood and drought years. In the flood years, the Jet is stronger over the northern Arabian Sea (AS) and weaker over the southern Bay of Bengal (BoB), favouring additional moisture transport and convergence over the Indian mainland, whereas reverse phenomena occur during drought years.

Examining the mean state of the climate systems, modulation of rainfall over the sub-continent of India (SCI), and associated intraseasonal variability, represented by the new generation of CMIP6 models during surplus and deficit monsoon years has not attracted much attention. The present study intends to analyse the representation of surplus and deficit conditions in the new generations CMIP6 and their associated systematic biases in the mean state of ISMR, the role of ISO during surplus/deficit monsoon years, and its associated air-sea interactions. The present study helps to understand the rendition of air-sea interactions on intraseasonal timescales during the surplus/deficit monsoon years in the CMIP6 models. Section 2 describes the data and methodology, in Sect. 3, performance of the CMIP6 models in simulating the ISM, mean states of surplus/deficit conditions, and air-sea interactions for surplus and deficit monsoon years on intraseasonal timescales are presented. Section 4 describes the summary and conclusions of the present study.

2 Data and methodology

2.1 Data

The present study employs the historical runs of GCMs from the CMIP6 (Eyring et al. 2016). The names of the

GCMs, modeling centers, resolutions, and ensemble members used in the present study are given in Table 1. These GCMs were selected based on the availability of climate variables, which are necessary to assess the ISM variations. Daily precipitation, winds, specific humidity, SST, energy, and radiative fluxes produced by CMIP6 models were used for the analysis period (1980–2014; <https://esgf-node.llnl.gov/search/cmip6/>). The historical runs of CMIP6 models are forced with the natural and anthropogenic forcings with minimal of trace gases (Eyring et al. 2016). To validate the model's outputs, Tropical Rainfall Measuring Mission (TRMM) 3B42 version-7 rainfall data for the period 1998 to 2014 (Huffman et al. 2007; https://disc.gsfc.nasa.gov/datasets/TRMM_3B42_Daily_7/) and daily rainfall from the Indian Meteorological Department (IMD) is used available at a spatial resolution of $0.25^\circ \times 0.25^\circ$ from the period 1901 to 2014 (Pai et al. 2014a, b; https://imd pune.gov.in/Clim_Pred_LRF_New/Grided_Data_Download.html). Daily rainfall estimates from ~ 6950 rain gauge stations across the country with varying observations periods were regridded to fixed spatial grids after applying standard quality checks by Pai et al. (2014a, b). The large-scale climatological features of rainfall over India derived from this dataset were consistent with those derived from IMD's previous rainfall data sets at $0.5^\circ \times 0.5^\circ$ and $1^\circ \times 1^\circ$ resolutions (Rajeevan et al. 2008). The daily vertical fields of specific humidity, zonal and meridional winds are obtained from ERA-interim reanalysis (Dee et al. 2011; <https://apps.ecmwf.int/datasets/data/interim-full-daily/>). Daily latent heat flux (LHF) obtained from the Modern Era Retrospective-Analysis for Research and Analysis (MERRA) reanalysis (Rienecker et al. 2011; https://disc.gsfc.nasa.gov/datasets/M2T1NXFLX_5.12.4/summary). The 3 days running means of TMI SST (Huffman et al. 2010) is used. All data sets are obtained from 1980 to 2014 except TRMM products (1998–2014).

2.2 Methodology

To evaluate the model's performance in representing the ISMR (rainfall over land is considered), Taylor's (2001) skill score for the models is evaluated by the Eq. (1):

$$SS = \frac{4(1 + R)}{(1 + R_0)(\sigma_f + 1/\sigma_f)^2} \quad (1)$$

The maximum possible correlation (here it is taken as 1), σ_f is the normalized standard deviations, and R is the pattern correlation between observational and CMIP6 models. High and low-performing models are identified

Table 1 Details of the 30 GCMs form CMIP6 group used in the present study

Source ID	Modeling Group and Country	Nominal resolution (lon×lat) Vertical levels	Ensemble member
ACCESS-CM2	Commonwealth Scientific and Industrial Research Organization and Bureau of Meteorology (Australia)	92°×144°, L85	r2i1p1f1
AWI-ESM-1-1-LR	Alfred Wegener Institute Climate Model (Germany)	192°×96°, L47	r1i1p1f1
BCC-CSM2-MR	Beijing Climate Center, China Meteorological Administration (China)	320°×160°, L46	r1i1p1f1
BCC-ESM1	Beijing Climate Center, China Meteorological Administration (China)	128°×64°, L26	r1i1p1f1
CanESM5	Canadian Centre for Climate Modelling and Analysis (Canada)	128°×64°, L49	r1i1p1f1
CESM2	National Science Foundation, Department of Energy, National Center for Atmospheric Research (Boulder)	288°×192°, L32	r1i1p1f1
CESM2-FV2	National Science Foundation, Department of Energy, National Center for Atmospheric Research (Boulder)	144°×96°, L32	r1i1p1f1
CESM2-WACCM	National Science Foundation, Department of Energy, National Center for Atmospheric Research (Boulder)	288°×192°, L70	r1i1p1f1
CESM2-WACCM-FV2	National Science Foundation, Department of Energy, National Center for Atmospheric Research (Boulder)	144°×96°, L70	r1i1p1f1
CNRM-CM6-1	Centre Européen de Recherche et de Formation Avancée en Calcul Scientifique (France)	128°×256°, L91	r2i1p1f2
CNRM-ESM2-1	Centre Européen de Recherche et de Formation Avancée en Calcul Scientifique (France)	128°×256°, L91	r1i1p1f2
EC-Earth3	European EC-Earth consortium with SMHI as coordinating partner	512°×256°, L91	r1i1p1f1
FGOALS-f3-L	LASG, Institute of Atmospheric Physics, Chinese Academy of Sciences and Center for Earth System Science, Tsinghua University (China)	360°×180°, L32	r1i1p1f1
FGOALS-g3	LASG, Institute of Atmospheric Physics, Chinese Academy of Sciences and Center for Earth System Science, Tsinghua University (China)	180°×80°, L26	r1i1p1f1
GFDL-CM4	Geophysical Fluid Dynamics Laboratory, USA	360°×180°, L33	r1i1p1f1
HadGEM3-GC31-LL	Met Office Hadley Centre	192°×144°, L85	r1i1p1f3
HadGEM3-GC31-MM	Met Office Hadley Centre	432°×324°, L85	r1i1p1f3
INM-CM4-8	Institute for Numerical Mathematics, Russian Academy of Science /Russia	180°×120°, L21	r1i1p1f1
INM-CM5-0	Institute for Numerical Mathematics, Russian Academy of Science /Russia	180°×120°, L73	r1i1p1f1
IPSL-CM6A-LR	L'Institut Pierre-Simon Laplace (France)	144°×143°, L79	r1i1p1f1
KACE-1-0-G	National Institute of Meteorological Sciences; Korea Meteorological Administration (Korea)	192°×144°, L85	r1i1p1f1
MIROC-ES2L	National Institute for Environmental Studies, The University of Tokyo (Japan)	128°×64°, L40	r1i1p1f2
MIROC6	National Institute for Environmental Studies, The University of Tokyo (Japan)	256°×128°, L81	r1i1p1f1
MPI-ESM-1-2-HAM	Max Planck Institute for Meteorology (Germany)	192°×96°, L47	r1i1p1f1
MPI-ESM-1-2-HR	Max Planck Institute for Meteorology (Germany)	384°×192°, L95	r1i1p1f1
MRI-ESM2-0	Meteorological Research Institute (Japan)	320°×160°, L80	r1i1p1f1
NorESM2-LM	Norwegian Climate Centre (Norway)	144°×96°, L32	r1i1p1f1
NorESM2-MM	Norwegian Climate Centre (Norway)	288°×192°, L32	r1i1p1f1
TaiESM1	Research Center for Environmental Changes (AS-RCEC) (Taiwan)	288°×192°, L30	r1i1p1f1
UKESM1-0-LL	Jointly developed by UK Met Office & UK universities, UK	192°×144°, L85	r1i1p1f2

based on the skill score to evaluate the ISM system's surplus and deficit monsoon conditions.

The inter-model spread of climatological precipitation, across BPM CMIP6 models at each grid point is analysed by the formula [Eq. 2; (Huang et al. 2020)]

$$\sigma_p = \sqrt{\frac{1}{N} \sum_{i=1}^N (P_{BPM,i} - P_{B-MME})^2} \tag{2}$$

where σ_p is spread of the models, N is the number of models, here it is 10. $P_{BPM,i}$ and P_{B-MME} represent the precipitation of the i th BPM and the multi-model ensemble mean of BPM, respectively.

The surplus (flood)/deficit (drought) monsoon years are identified by averaging the rainfall (anomalies) during the summer monsoon season over the SCI, values are normalized by their own standard deviation, also known as standardized precipitation index (SPI; Goswami 2005; Krishnan et al. 2009; Saha et al. 2010). The surplus (deficit) monsoon years are identified with the normalized seasonal mean rainfall anomaly above (below) +0.75 (− 0.75). However, the percent of normal precipitation (PNP) index is the most common indices used to identify the surplus/deficit years of the monsoon (Mishra and Singh 2010; Pai et al. 2011, 2017). A PNP criterion was also analysed in the present study to identify the surplus and deficit monsoon years. PNP index is defined as the ratio of cumulative rainfall of the season to the long-term mean rainfall of the season multiplied by 100. The flood/drought years are considered as $\pm 10\%$ departure of rainfall from the mean (Fig. 2). An analysis is carried over the four major rainfall regions of ISM such as BoB (85°E–95°E, 5°N–20°N), AS (63°E–73°E, 5°N–20°N), SCI (74°E–84°E, 5°N–35°N), North Indian Ocean (NIO; 60°E–100°E, Equator–30°N), and eastern equatorial Indian Ocean (EEq IO; 75°E–100°E, 10°S–5°N) (Roxy et al. 2013; Goswami et al. 2016; Konda and Vissa 2021). The daily anomalies are estimated from the daily climatological means (first three harmonics removed). A 20–100 day Lanczos bandpass filter (Duchon 1979) is applied to the daily anomalies to acquire the intraseasonal variability. The present analysis is carried out for the Indian summer monsoon season (June to September).

The following Eq. (3) estimates vertically integrated moisture transport (VIMT):

$$VIMT = \frac{1}{g} \int_{P_{500}}^{P_{surface}} qVdp \tag{3}$$

where, g is the acceleration due to gravity, q is the specific humidity, and V is the horizontal velocity.

The phase speed of convection is estimated for each time-latitude section over the entire region (63°E to 95°E) longitudes by averaging the regressed precipitation anomalies across the latitude bands from 5°S to 30°N with an interval of 5°. For each latitudinal band, the time when the maxima occurred is considered. The speed of the northward propagation of convection is evaluated by the linear least-square fit on the time in which a maximum occurs within each latitude

band. Similarly, the phase speed of eastward convection is estimated for the longitudinal bands of 45°E to 140°E with an interval of 5° (Karmakar and Misra 2019).

3 Results

3.1 Performance of the CMIP6 models in representing the ISM

The representation of all ISMR is analysed in the 30 GCMs from the CMIP6 group by using Taylor’s skill score (SS), normalized standard deviation (NSTD), and normalized root mean square error (NRMSE). The majority of the models capture the precipitation patterns over the SCI with systematic biases. Figure 1a shows the statistics for the ISMR of 30 CMIP6 models. Most of the models show the $SS > 0.7$ with $NRMSE < 0.7$, however, some models (ACCESS-CM2, CanESM5, FGOALS-g3, IPSL-CM6A-LR, and MEI-ESM2-0) fail to simulate the seasonal mean precipitation over the mainland of India. The performance of the models in simulating the seasonal mean (area averaged cumulative rainfall over India) rainfall is analysed in the historical simulations (1980–2014) of 30 GCMs from the CMIP6 group (Fig. 1b). In the observations (IMD, Pai et al. 2011), the cumulative mean rainfall is 852.6 mm, and the coefficient of variation (CV) is about 8.6% (Kripalani et al. 2007; Preethi et al. 2019; Rajendran et al. 2021). However, models show the uncertainties in simulating the seasonal mean rainfall over India vary from 976.16 mm (INM-CM4-8) to 399.89 mm (CanESM5), and CV varies from 26.41% (CanEsm5) to 7.48% (MIROC-ES2L). The new generation of CMIP6 models shows a significant improvement in representing the seasonal mean precipitation over India compared to the CMIP5 models (Preethi et al. 2019; Gusain et al. 2020; Rajendran et al. 2021). INM-CM5-0 and TaiESM1 models shows the good agreement with the observations in representing the mean precipitation over the mainland of India. 43% of models reasonably well simulated the seasonal mean precipitation (above 650 mm) and CV (below 15%), and 20% of models show the mean precipitation above 800 mm (Fig. 1b). The presence of uncertainties in the simulation of mean precipitation among the models impacts the monsoon’s intraseasonal and inter-annual variability. Best performing models (BPM) are identified in simulating the seasonal mean precipitation over the India, based on the statistics of $SS (> 0.7)$, $NRMSE (< 0.7)$, $NSTD$ (close to 1), mean ISMR (> 650 mm), and $CV (< 15\%)$ (Kripalani et al. 2007; Preethi et al. 2019). Based on the above criteria, 10 (AWI-ESM-1-1-LR, BCC-CSM2-MR, BCC-ESM1, CNRM-CM6-1, CNRM-ESM2-1, GFDL-CM4, INM-CM5-0, MIROC-ES2L, MIROC6, TaiESM1) models are considered as BPM (Fig. 1). Further, the MME of BPM

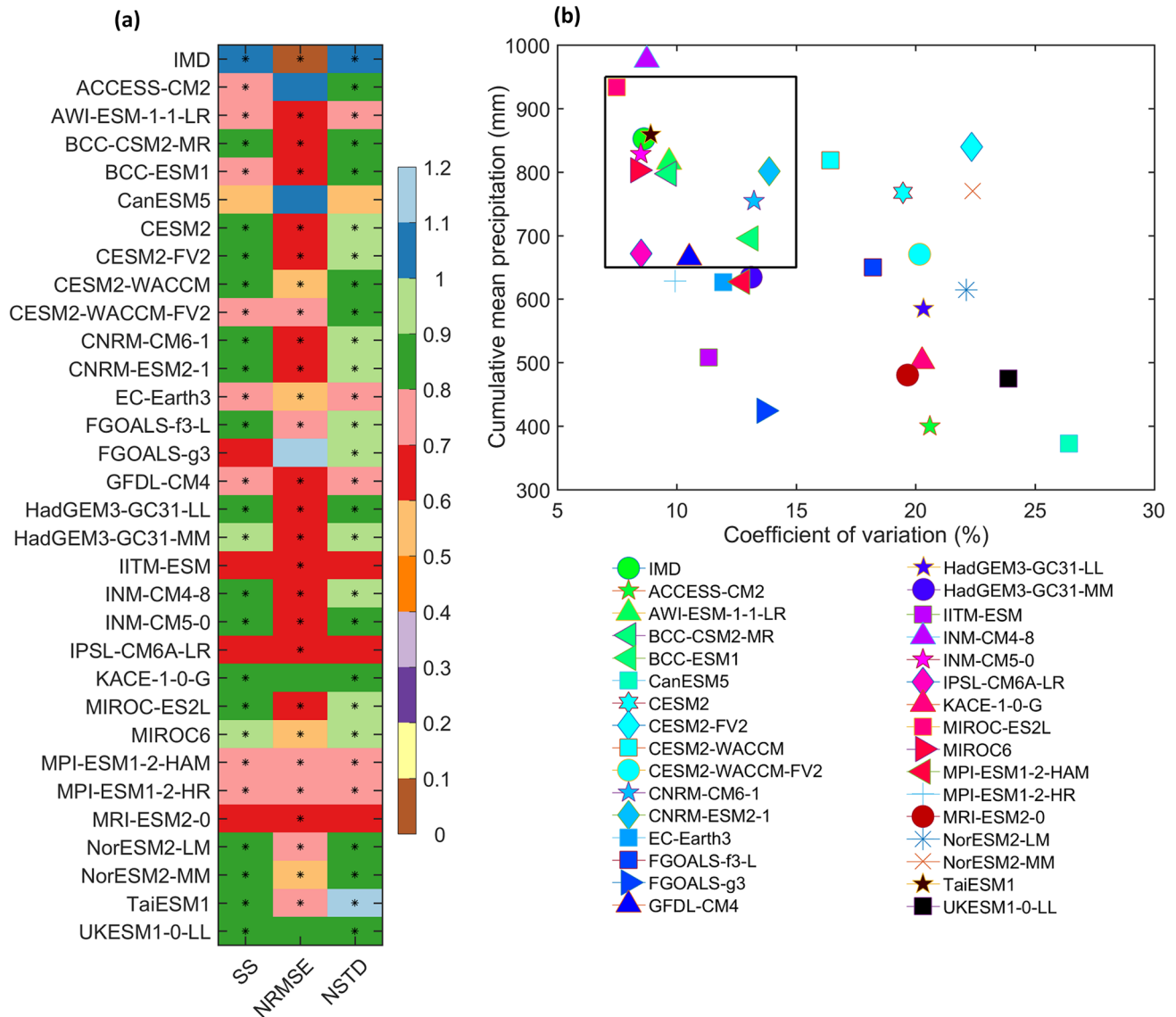


Fig. 1 **a** Diagram metric for statistics (Taylor skill score, normalized standard deviation and root mean square error) for all India mean (JJAS; 1980–2014) precipitation, **b** cumulative mean precipitation

(mm) and coefficient of variation (%) for the observations (IMD) and historical simulations of 30 CMIP6 models. Models satisfied the criteria are indicated with *

models (hereafter B-MME) is analysed in representing the ISMR. The mean ISMR simulated by the B-MME is about 798.42 mm, and its associated CV is about 10.2%.

3.2 Mean state and surplus/deficit monsoon years

The rendition of surplus and deficit conditions in the new generation of coupled GCMs is analysed. All India surplus and deficit monsoons are identified using the PNP and the SPI criteria’s in the observations and B-MME (Fig. 2). The seasonal mean precipitation shows the large variability over the Indian mainland (Fig. 2b). The large spread of the seasonal mean precipitation is associated with the strong

underestimation of precipitation compared to the observations (Fig. 2a). The median values also show a strong interannual variability of the monsoonal precipitation over the Indian mainland. It is identified that the intermodel spread of climatological precipitation (Fig. 2c) tends to be larger over the regions with large rainfall amounts and mean biases, typically concentrated over the Western Ghats and east Indian region. Surplus/deficit monsoon years are considered for the composite analysis are given in Table 2. The seasonal mean rainfall shows a high rainfall over central and northeast India (Fig. 3a). B-MME is able to capture the similar rainfall pattern compared with the observations (SS is 0.76 and NRMSE is 0.45).

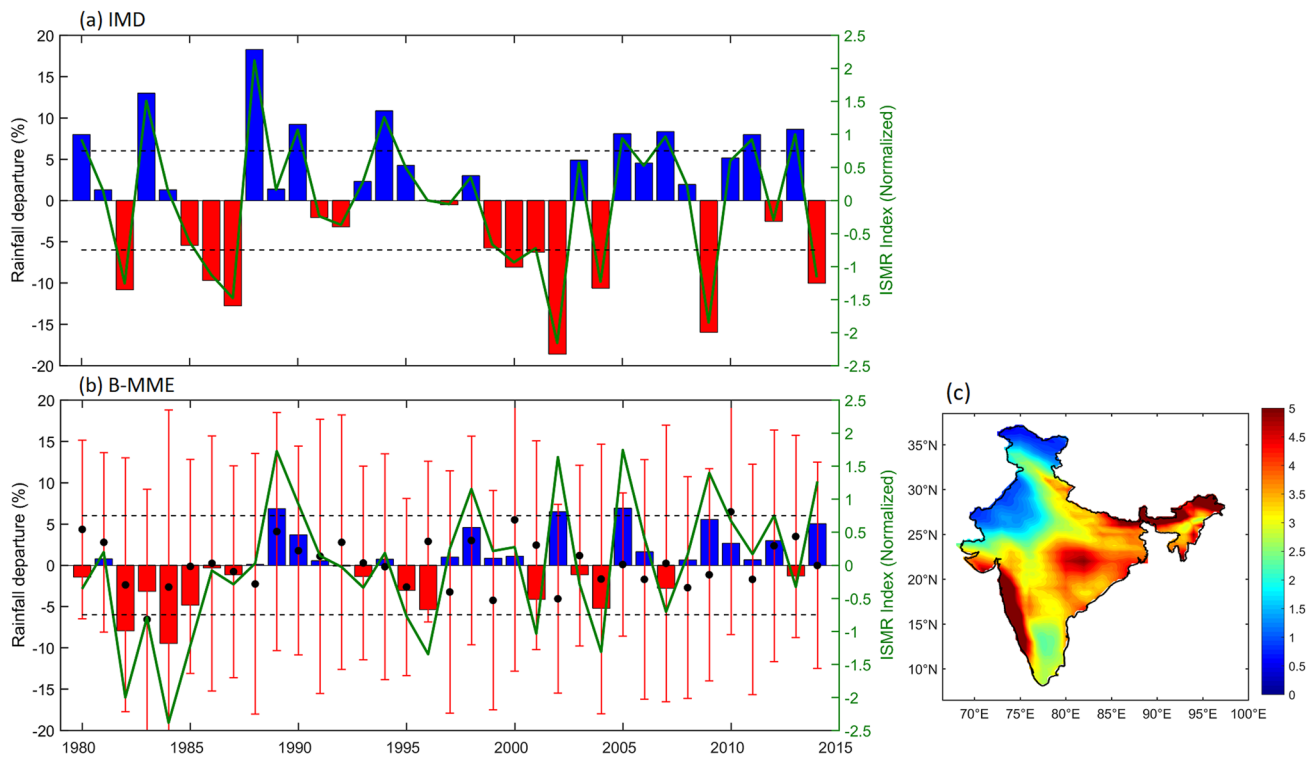


Fig. 2 All India summer monsoon precipitation departure (%) from the long-term mean (1980–2014), using PNP criteria (positive departure in blue color bars and negative departure in red color bars). Solid thick line (green) represents the SPI criteria and dashed line represents the ± 0.75 SPI values. The intermodal spread of the best performing models (BPM) models is shown by black points in each bar

for the median values of ISMR index, the vertical lines in red color indicates one standard deviation centered around the point. **a** for IMD and **b** for B-MME. The inter-model spread of BPM CMIP6 models in simulating climatological mean precipitation (color filled) for the Indian monsoon season (**c**)

Table 2 Excess and deficit Indian summer monsoon years simulated by CMIP6 BPM models and B-MME

Models	Excess monsoon years	Deficit monsoon years
AWI-ESM-1-1-LR	1989, 1990, 1998, 2000, 2004, 2007, 2008, 2010	1982, 1996, 2001, 2003, 2009, 2012
BCC-CSM2-MR	1988, 1989, 1990, 1997, 1998, 2008, 2009	1983, 1984, 1987, 1991, 1992, 1995, 1999, 2014
BCC-ESM1	1981, 1993, 1998, 2000, 2001, 2005, 2014	1984, 1985, 1989, 1990, 1991, 1997, 2003, 2004, 2007, 2010
CNRM-CM6-1	1989, 1990, 1991, 1992, 1998, 2002, 2004, 2010, 2012	1981, 1982, 1984, 1986, 1993, 1999, 2000, 2001
CNRM-ESM2-1	1983, 1989, 1991, 1994, 2002, 2011, 2012	1982, 1984, 1985, 1997, 1998, 2004, 2008, 2010
GFDL-CM4	1990, 1999, 2002, 2003, 2005, 2006, 2009	1980, 1986, 1988, 1991, 1992, 1994, 2000, 2007
INM-CM5-0	1984, 1985, 1989, 1993, 1998, 1999, 2004, 2009, 2010, 2014	1981, 1982, 1983, 1988, 1990, 1991
MIROC-ES2L	1983, 1986, 1992, 1997, 1998, 2002, 2005, 2006, 2007, 2012	1980, 1982, 1984, 1985, 1989, 1996, 2003, 2004, 2010, 2013, 2014
MIROC6	1981, 1985, 1987, 1988, 1989, 2000, 2005, 2010, 2014	1982, 1983, 1984, 1993, 1999, 200, 2013
TaiESM1	1986, 1988, 1991, 1999, 2009, 2010, 2014	1983, 1987, 2004, 2007, 2008
B-MME	1989, 1990, 1998, 2002, 2005, 2009, 2012, 2014	1982, 1983, 1984, 1985, 1995, 1996, 2001, 2004

However, B-MME shows significant dry biases over the Western Ghats, northwest India, and the foothills of the Himalayan Mountains (Fig. 3g). B-MME overestimates the precipitation over the leeward side of the Western

Ghats, which suggests that models are fail to represent the orographic precipitation. Models that overestimate the precipitation along the east coast of India could be associated with the local convective systems, suggesting

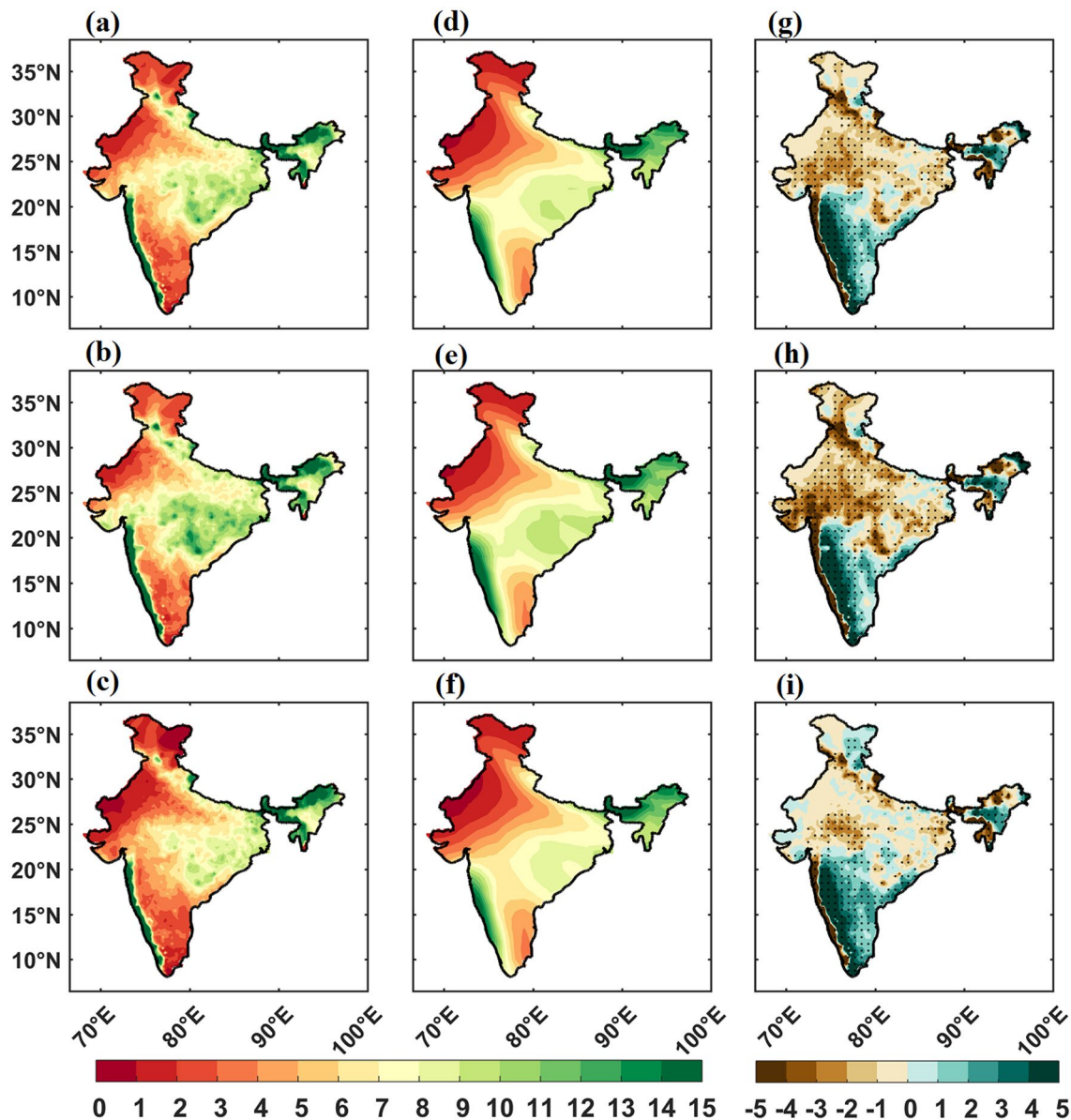


Fig. 3 **a** JJAS seasonal mean, **b** composite of surplus monsoon, **c** composite of deficit monsoon precipitation (mm day^{-1}) for IMD, **d–f** is same as of **a–c** but for B-MME, **g–i** represents the biases (B-MME-

IMD) of seasonal mean, surplus, and deficit monsoon composites respectively. Areas of 95% significant level are masked with ‘.’

that models simulate the strong convective systems along the east coast of India. The surplus/deficit monsoon composite analysis revealed that B-MME is able to capture the precipitation patterns; however, significant biases are observed. B-MME replicates the biases pattern similar to the seasonal mean (Fig. 3h) with significant strong biases during surplus composite. During deficit monsoon composite, B-MME overestimates the rainfall over the leeward side of the Western Ghats and the regions of central India (Fig. 3i). Precipitation activity over SCI is directly linked to the amount of moisture transport from the surrounding oceans (Swapna and Ramesh Kumar 2002; Levine and

Turner 2012; Patil et al. 2019). The significant biases in precipitation are further analysed with the moisture transport (Fig. 3).

The seasonal mean of moisture transport (Fig. 4) reveals that B-MME captures the mean features of moisture transport from the West Indian Ocean (WIO) to the mainland of India. However, B-MME overestimates the moisture over south peninsular India, and underestimation is evident over central India and the equatorial Indian Ocean (Fig. 4g). During surplus monsoon years, strong moisture transport is evident from the AS to the mainland of India, compared to the deficit monsoon years. A large amount of moisture transport

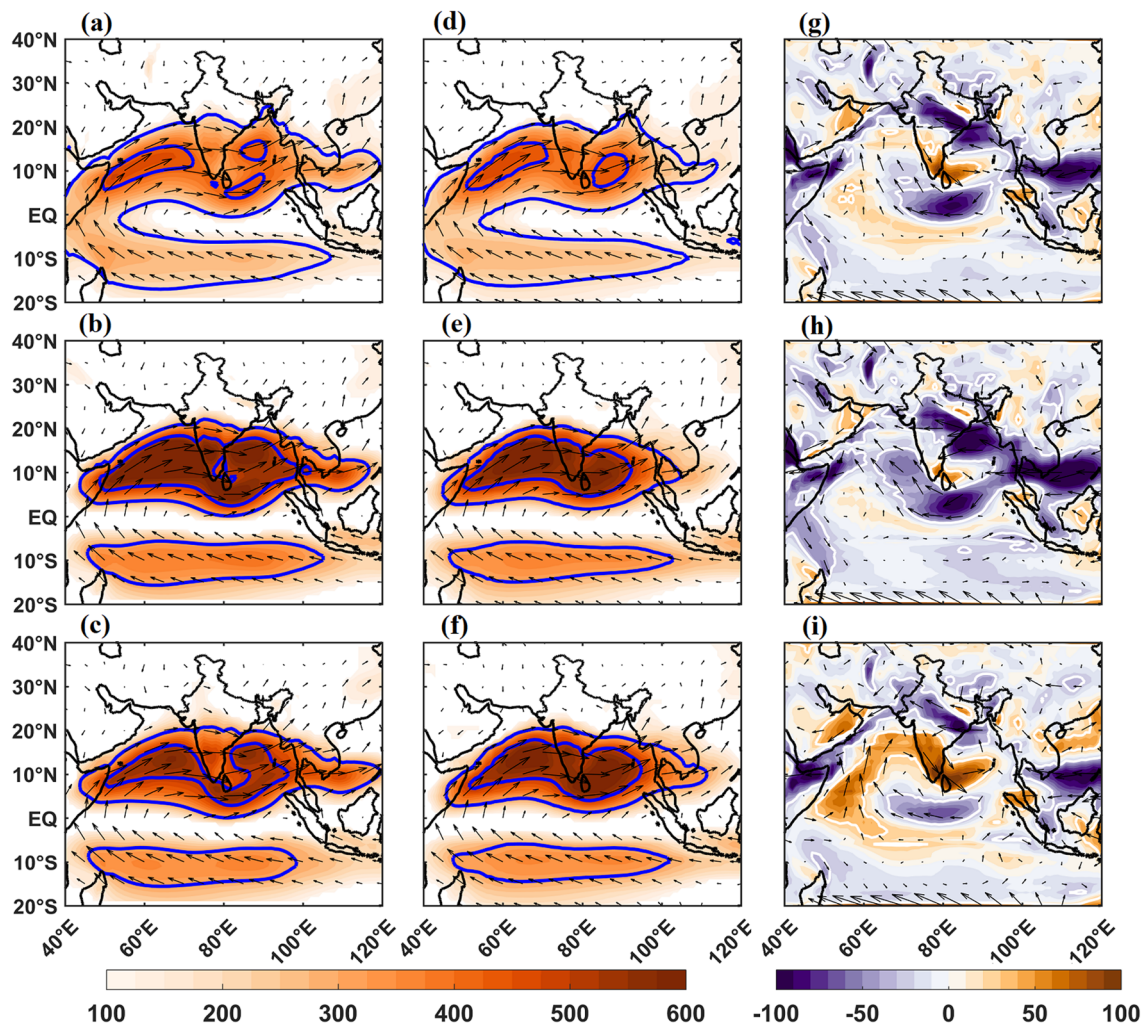


Fig. 4 Same as of Fig. 3, but for moisture transport (shaded; $\text{kg m}^{-1} \text{s}^{-1}$) and vectors (direction). Outer and inner contours (left and middle panels) represent the 500 and 300 $\text{kg m}^{-1} \text{s}^{-1}$ respectively. White contours in g–i represent the areas of 95% significance

and associated high wind speed contributes to the widespread moisture transport during surplus monsoon years. These results are consistent with Patil et al. (2019). In the observations, the strong moisture transport ($300 \text{ kg m}^{-1} \text{s}^{-1}$ contours) is extended up to the west Pacific (120°E); however, this transport is limited to the 110°E in the B-MME (Fig. 4d). The surplus monsoon composite of moisture transport reveals that B-MME is able to capture the strong moisture transport from WIO to the mainland of India; however, a large underestimation of moisture is observed in the regions of the west coast of the Indian Ocean, AS, and north BoB (Fig. 4h). During deficit monsoon composite, strong moisture transport ($500 \text{ kg m}^{-1} \text{s}^{-1}$ contours) is seen from AS to BoB; however, B-MME overestimates the moisture transport (Fig. 4i). This strong moisture transport in the B-MME is responsible for the wet biases of precipitation during the deficit monsoon composite over southern India. Biases in precipitation simulated by the models have primarily been

due to the simulation of SST, low-level winds, and the spatial resolution of the models (Yang et al. 2019; Pathak et al. 2019). Improving the simulations of low-level winds and SST would better agree on India's surplus/deficit monsoon conditions.

The composite anomaly of precipitation for the surplus/deficit monsoon years is shown in Fig. S1. B-MME can capture the wet and dry anomalies of precipitation over the parts of India compared to the observations; however, B-MME fails to represent the precipitation over the northeast regions of India. A composite of SST anomalies is shown in Fig. S2. During surplus monsoon, observations show the warming of SST in the western equatorial Indian Ocean and cooling in the central AS and southern Indian Ocean (Fig. S2a) represents the positive IOD-like pattern (Ashok et al. 2001; Cherchi and Navarra 2013). B-MME shows significant warming over large parts of the Indian Ocean as compared to observations. B-MME fails to capture the southern Indian Ocean

cooling during surplus monsoon. During deficit monsoon years, observations show the negative IOD-like pattern, and B-MME can capture the cooling over the WIO and warming in the Sumatra region with weak anomalies. In consistent with the observations B-MME captures the La Niña conditions during surplus monsoon years, however B-MME fail to capture the El Niño conditions over the eastern Pacific Ocean during deficit monsoon years. Composite anomalies of moisture during surplus and deficit monsoons are shown in Fig. S3. During surplus monsoon, strong moisture transport is evident from AS to the mainland of India. The cyclonic circulation over central India draws the moisture from AS, leading to the active spells of monsoonal rainfall (Fig. S3a). B-MME shows the strong westerlies from the African coast and easterlies from the northwest Pacific Ocean converge over the mainland of India, forming the cyclonic circulation over central India. However, the cyclonic circulation center is shifted northwestward compared to the observations. B-MME underestimates the southwesterly from WIO to the SCI (Fig. S3c). During deficit monsoon composite, in the observations, strong anticyclonic circulation is evident over central India, and cyclonic circulation is observed over AS. These anticyclonic and cyclonic circulations favor the monsoon's break spells, leading to the deficit of monsoonal

rainfall (Fig. S3b). B-MME fails to capture the circulation patterns as compared to the observations. The misrepresentation of SST and moisture transport in the B-MME is responsible for the significant precipitation biases over the Indian mainland during surplus and deficit monsoon years (Fig. S1).

3.3 Intraseasonal variations of air-sea interactions during surplus and deficit monsoons

The ISMR exhibits strong intraseasonal variability (Annamalai and Slingo 2001; Waliser et al. 2003; Waliser 2006; Goswami et al. 2014; Zhou and Murtugudde 2014), and the precipitation anomalies associated with the 20–100 day (intraseasonal) propagate eastward and northward. It is essential to analyze the representation of intraseasonal variations of monsoonal precipitation during surplus/deficit monsoon years in the observations and B-MME. Figure 5 represents the northward propagation of convection for the monsoon season, surplus, and deficit monsoon. To evaluate the northward propagation of convection, longitudinally (63°N to 95°N) averaged 20–100 day bandpass filtered precipitation anomalies are regressed against the area (12°N–22°N and 70°E–90°E) averaged filtered precipitation

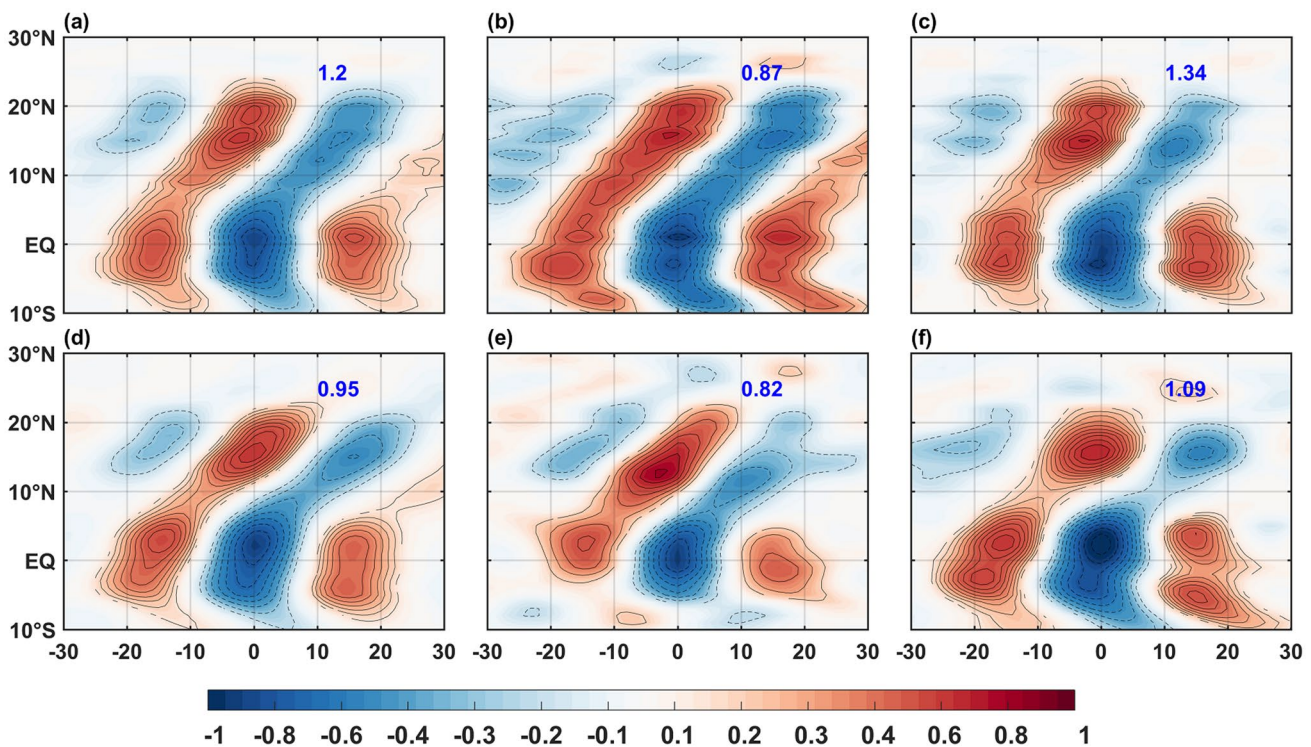


Fig. 5 Lag-latitude diagram of northward propagating convection for the monsoon season (a), surplus (b) and deficit (c) for observations (TRMM; mm day⁻¹). d–f for the B-MME. Each diagram is obtained as lead-lag regression of longitudinally (63°E to 95°E) averaged intra-

seasonal precipitation anomalies regressed against its time series averaged over 70°E–90°E, 12°N–22°N. Blue values in each diagram represent the phase speed. Solid and dashed contours represent the 95% significant values (0.05 significance level using *t* test)

anomalies (Sabeerali et al. 2013; Konda and Vissa 2021). On intraseasonal timescales, convection originated in the equatorial Indian Ocean and propagates northward to the SCI with a phase speed of $1.2^\circ\text{lat}/\text{day}$ (Fig. 5a) (Wang et al. 2018; Karmakar and Mishra 2020). During surplus monsoon years, the convection anomalies propagate slowly ($0.87^\circ\text{lat}/\text{day}$) when compared with the deficit monsoon years ($1.34^\circ\text{lat}/\text{day}$) (Fig. 5b and c). However, the magnitude of convection anomalies is strong in the surplus monsoon years. The sluggish propagation of convection anomalies leads to a longer duration of convective activity and causes heavy precipitation over the region. However, B-MME captured the northward propagation of convection anomalies with a phase speed $0.95^\circ\text{lat}/\text{day}$ (seasonal mean; Fig. 5d). During surplus (deficit) monsoon, B-MME shows the phase speed of 0.82 (1.09) $^\circ\text{lat}/\text{day}$ (Fig. 5e and f). B-MME can capture the phase speed differences between surplus and deficit monsoon years compared to the observations; however, B-MME underestimates the phase speed of convection anomalies. The eastward propagation of convection anomalies is obtained by averaging the anomalies over the latitudes of 10°S – 10°N , and these anomalies are regressed against the area (10°S – 5°N and 75°E – 100°E) averaged filtered precipitation anomalies (Ahn et al. 2020) (Fig. 6). The seasonal

mean state shows the propagation of strong convection anomalies from the Indian Ocean to the west Pacific Ocean with a phase speed of $4.13^\circ\text{lon}/\text{day}$ (Fig. 6a) (Jiang et al. 2004; Neena et al. 2017). During surplus (deficit) monsoon, weak (strong) anomalies are observed in the western Pacific Ocean. The phase speed analysis reveals that, during surplus (deficit) monsoon years, precipitation shows the sluggish (quick) propagation to the western Pacific with a phase speed of 3.48 (4.18) $^\circ\text{lon}/\text{day}$. The sluggish propagation of convection favors the long duration of convective activity and leads to more precipitation over the Indian longitudes. B-MME models are able to capture the features of eastward propagating convection activity during surplus and deficit monsoon years compared with the observations. However, models overestimate (underestimate) the phase speed of convection anomalies during surplus (deficit) monsoon. The phase speed of the convection is governed by the moisture gradient (Sobel et al. 2001; Jiang et al. 2004). Stronger (weaker) north–south gradient of moisture strengthened (weakened) the phase speed of convection on intraseasonal timescales (Jiang et al. 2004; Yamaura and Kajikawa 2017) and the enhanced air-sea fluxes ahead of the convection center favoring fast movement of the convection (DeMott et al. 2016; Gao et al. 2019).

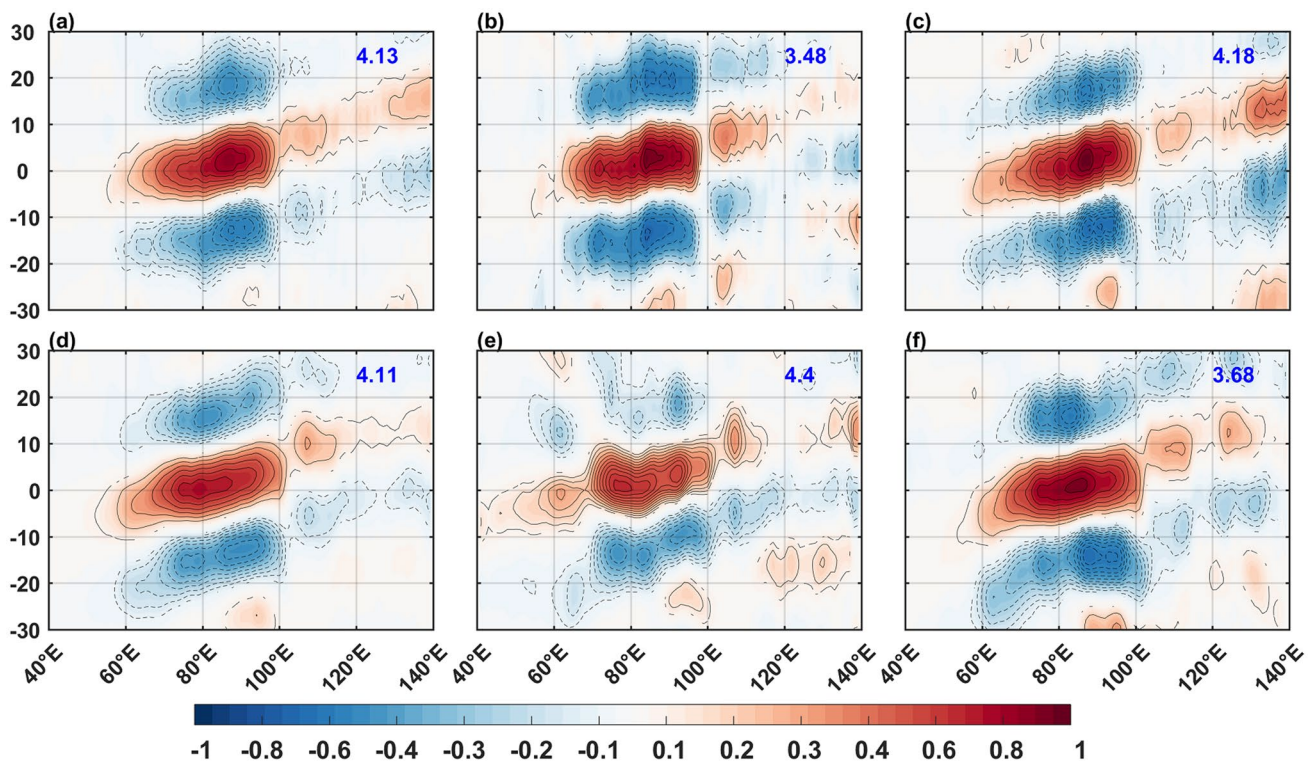


Fig. 6 Lag-longitude diagram of eastward propagating convection for the monsoon season (a), surplus (b) and deficit (c) for observations (TRMM; mm day^{-1}). d–f for the B-MME. Each diagram is obtained as lead-lag regression of latitudinal (-10°S to 10°N) averaged intra-

seasonal precipitation anomalies regressed against its time series averaged over 75°E – 100°E , 15°S – 5°N . Blue values in each diagram represent the phase speed. Solid and dashed contours represent the 95% significant values (0.05 significance level using t-test)

The phase relationship of air-sea fluxes on intraseasonal timescales in B-MME is evaluated during surplus/deficit monsoon years over the North Indian Ocean region with the observations. On intraseasonal timescales, underlying SST and the exchange of energy fluxes play a vital role in the propagation and maintenance of convection (Shinoda et al. 1998; Sengupta et al. 2001; Jinag et al. 2004; Roxy and Tanimoto 2007; DeMott et al. 2013; Roxy et al. 2013; Gao et al. 2019; Karmakar and Misra 2020; Konda and Vissa 2019, 2021). Singh and Dasgupta (2017) analysed the AS and BoB response to the rainfall over India on different intraseasonal timescales during strong/weak monsoon years. Ocean response to atmosphere and vice-versa are revealed using the lead-lag correlation (± 20 days) over the sub-regions (AS, BoB, SCI, NIO, and EEq IO) during the surplus and deficit monsoon years. Correlation values represent the strong/weak response, and lead/lag days represent the response time between them. On intraseasonal timescales, during monsoon season, SST leads precipitation by 5 and 12 days over AS and BoB (Roxy et al. 2013; Konda and Vissa 2021). The phase relationship of SST and precipitation over AS, BoB, NIO, and EEq IO is shown in Fig. 7. Over AS, during surplus (deficit) monsoon years, SST leads precipitation by ~ 6 (~ 8) days. The strong response from the ocean to the atmosphere is observed during the deficit monsoon years, is associated with the less cloud coverage over the basin (Shinoda et al.

1998; Roxy et al. 2013; Konda and Vissa 2019) and the weakening of southwesterly from the AS to the SCI during deficit monsoon years supports the further warming of the basin (Hendon 2005; DeMott et al. 2015) leading to increase of SST. During surplus monsoon years, ocean to atmosphere response is weak is associated with the strong convection and monsoonal winds over the basin. However, the atmosphere-to-ocean response is quick (slow) during deficit (surplus) monsoon years. B-MME shows the slow response from the ocean to the atmosphere during surplus and deficit monsoons. CNRM-CM6-1 model fails (correlations are insignificant; Fig. S4) to capture the response between ocean and atmosphere over all the regions. Over BoB, the response from the ocean to the atmosphere is weak and quick (correlation 0.45 at ~ 7 days) in the deficit monsoon years. However strong response (correlation is 0.52 at ~ 12 days) is evident during surplus monsoon years. The strong response from ocean to atmosphere in the BoB during surplus monsoon years is associated with the influx of freshwater into the BoB (Thadathil et al. 2002; Shenoi et al. 2002; Mahadevan et al. 2016), causes the warming at the surface leads to a strong response to the atmosphere (Goswami et al. 2016). However, B-MME shows strong (weak) response in the surplus (deficit) monsoon years. Over NIO, B-MME shows the slow response compared to the observations, and B-MME fails to capture the ocean and atmosphere response during deficit monsoon.

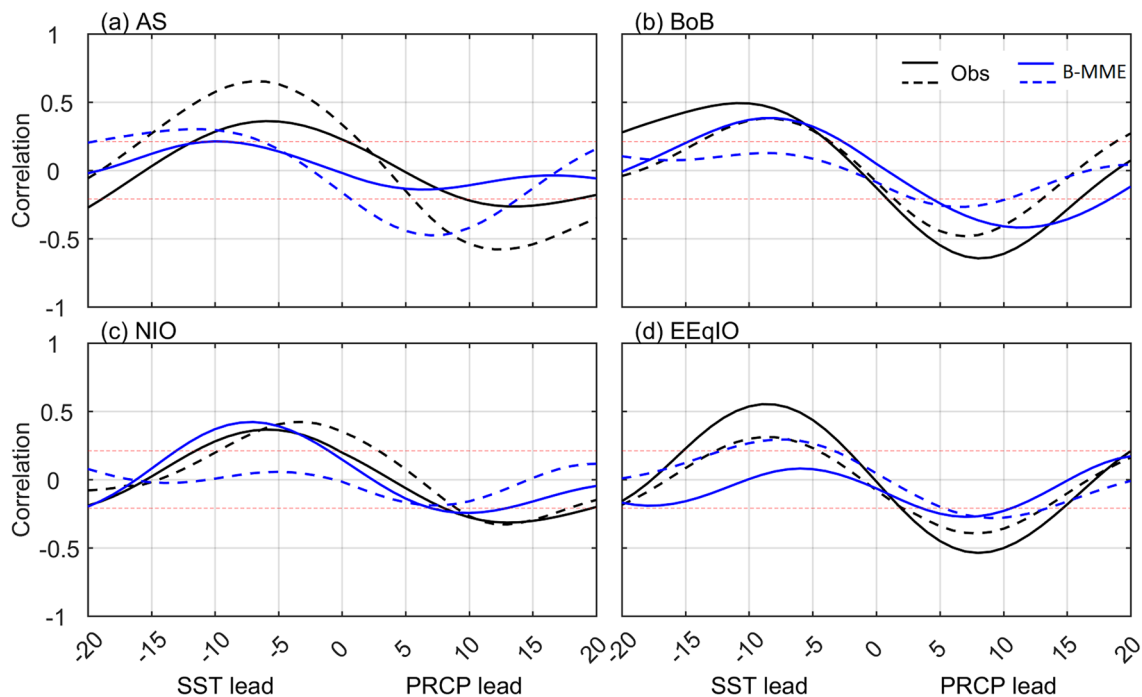


Fig. 7 Intraseasonal Ocean and atmosphere response (lead-lag cross-correlation) for surplus (solid) and deficit (dashed) monsoon years in the observations, B-MME of models. Lead-lag cross-correlation of

SST and precipitation anomalies averaged over AS (a), BoB (b), NIO (c), and EEq IO (d). Correlation values are statistically significant (red lines; 0.05 significance level using *t* test)

In the EEq IO, a significant response from the ocean to the atmosphere is observed during surplus monsoon years.

The phase response of SST and U850 is shown in Fig. 8. On intraseasonal timescales, easterlies lead warmer SST over AS, BoB, NIO, and EEq IO by ~ 6 , ~ 3 , ~ 7 , and ~ 3 days, respectively. However, the CNRM group of models are fail to represent the phase response of SST and U850 over all the regions (Figure not shown). During deficit monsoon years, the response between easterlies to the SST is strong over AS, GFDL-CM4, and MIROC6 models are able to capture the phase response of U850 and SST; B-MME shows the insignificant correlation of U850 and SST over the regions except for EEq IO. This could be associated with the underestimation of low-level winds by the models. Over BoB, quick (~ 3 days) response of U850 to SST is evident compared to the AS, and models show the slow and weak response between them compared to the observations. Over the NIO, GFDL-CM4 and MIROC6 models can capture the in-phase relationship of U850 and SST. MIROC6 model well represented the in-phase relationship over all the regions. The response of U850 and precipitation is shown in Fig. 8. Westerlies lead precipitation over AS and BoB by ~ 8 and ~ 5 days (Fig. 9a, b). However, models show the quick response between U850 and precipitation. In the observations, there is no significant differences between U850 and precipitation response time and intensity during surplus and deficit monsoons over AS, BoB, and NIO. CNRM-ESM2-1 and

MIROC-ES2L models are fail to represent the in-phase relationship of U850 and precipitation over all the regions. Over SCI, westerlies lead precipitation by ~ 6 (~ 10) days during deficit (surplus) monsoon years. B-MME fails to capture the in-phase relationship of U850 and precipitation over SCI.

It is essential to analyse the phase response between DSSR and SST (Fig. 10). DSSR leads warmer SST on intraseasonal timescales by ~ 7 , ~ 5 , and ~ 8 days over AS, BoB, and EEq IO, respectively. B-MME is able to capture the phase relationship of DSSR and SST over AS and NIO and fails to represent over BoB and EEq IO. Models (except CNRM-CM6-1 and INM-CM5-0) show the in-phase relationship of DSSR with the SST over the regions (Fig. S6). However, over BoB, during surplus monsoon years, the strong response from DSSR to the warmer SST is evident, influencing the precipitation response to the SST. Overall the regions (except EEq IO) models show a solid and quick response between DSSR and precipitation (Fig. S5). The response of latent heat flux to the precipitation is analysed (Fig not shown). Significant correlations are found over BoB. During the convection process, low-level specific humidity (SHUM) plays a vital role (Zheng and Huang 2019). Understanding ISO dynamics is necessary to properly represent the phase relationship between low-level SHUM (vertically integrated from surface to 500 hPa) with precipitation. The phase association of SHUM-precipitations is analysed (Fig. S7). Overall the regions (except BoB) SHUM

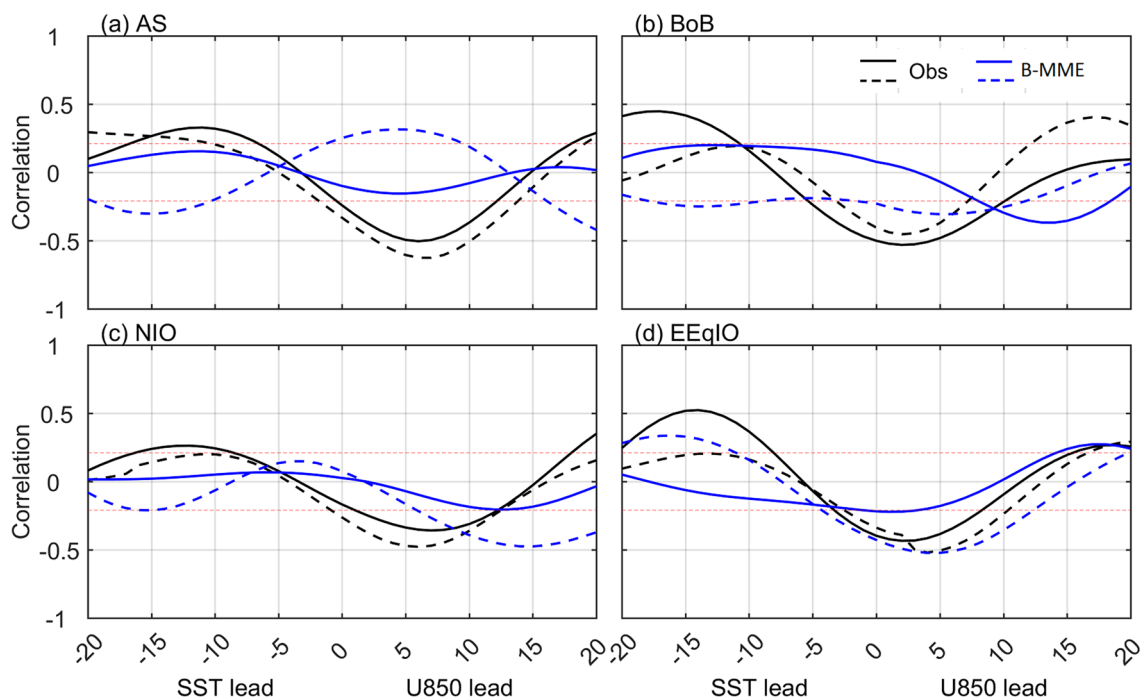


Fig. 8 Intraseasonal Ocean and atmosphere response (lead-lag cross-correlation) for surplus (solid) and deficit (dashed) monsoon years in the observations, B-MME of models. Lead-lag cross-correlation of

SST and U850 anomalies averaged over AS (a), BoB (b), NIO (c), and EEq IO (d). Correlation values are statistically significant (red lines; 0.05 significance level using *t* test)

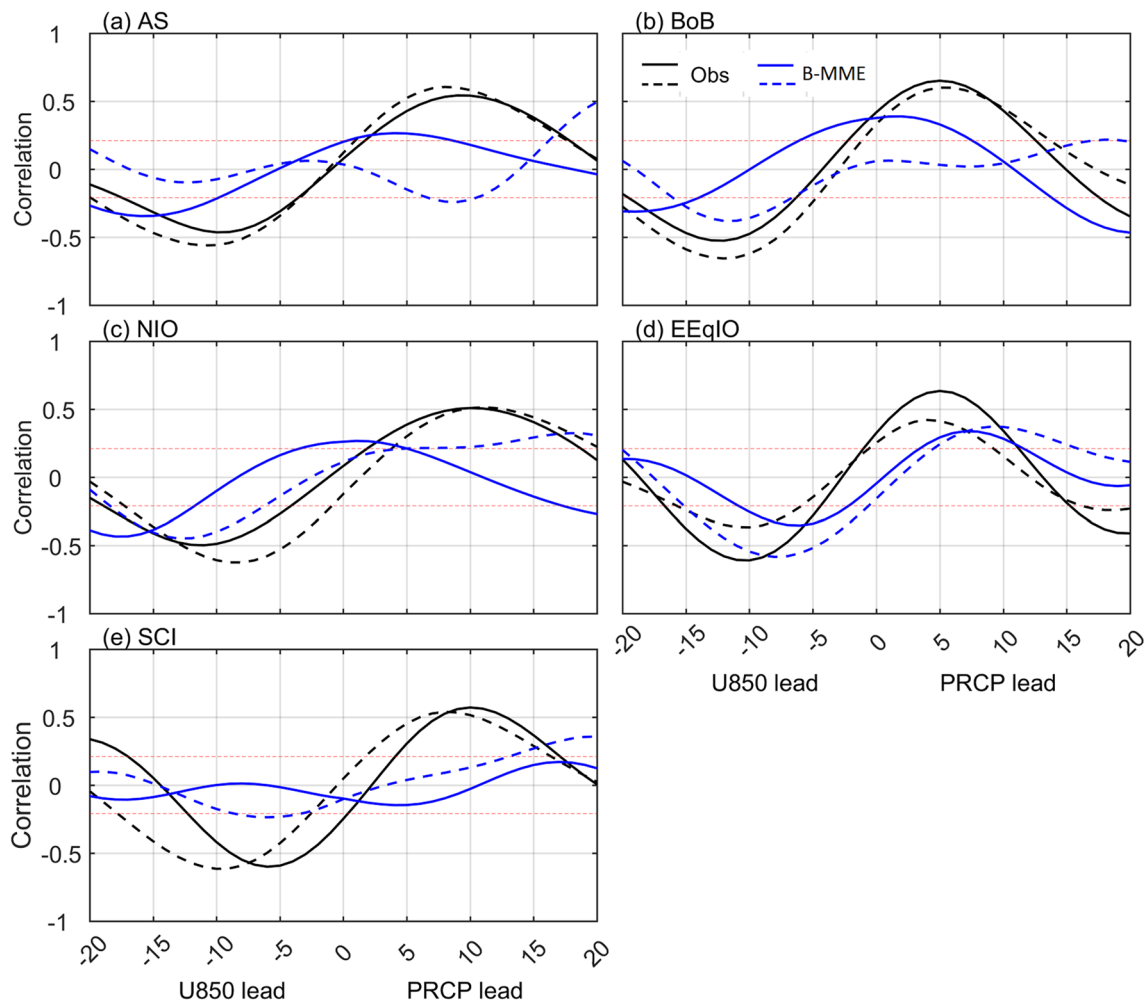


Fig. 9 Intraseasonal response (lead-lag cross-correlation) for surplus (solid) and deficit (dashed) monsoon years in the observations, B-MME models. Lead-lag cross-correlation of U850 and precipita-

tion anomalies averaged over AS (a), BoB (b), NIO (c), EEq IO (d), and SCI (e). Correlation values are statistically significant (red lines; 0.05 significance level using *t* test)

and precipitation show the in-phase association. Over BoB, SHUM leads precipitation by 2 days. CNRM-ESM2-1 model fails to capture the response time between SHUM and precipitation compared to the observations. Over SCI, the strong (weak) response between SHUM and precipitation is evident during deficit (surplus) monsoon years.

4 Summary and conclusions

This study aimed to evaluate the performance of CMIP6 models in simulating the surplus/deficit seasonal monsoon rainfall and the association of air-sea interactions on intraseasonal timescales over the India and adjoining oceans. The majority of the CMIP6 models simulate the ISMR with good skill scores; however, systematic biases exist. The majority of the CMIP6 models are able to capture the cumulative mean rainfall over the mainland of India.

The precipitation biases in the model simulations are primarily due to the simulation of SST, low-level winds, moisture transport from the WIO to the mainland, and the spatial resolution of the models. However, improving the simulations of low-level winds and SST with high spatial resolutions would better agree on the historical and future projections. BPM models are identified to analyse the existence of biases in association with the surplus/deficit monsoons. The B-MME outperforms the simulation of ISMR with weak biases. The overall enactment in simulating the ISMR by B-MME is about 798.42 mm, and its associated CV is about 10.2%. The seasonal mean precipitation analysis suggests that, B-MME failed in representing the orographic precipitation and overestimate the local convective activity over the east coast of India. Significant biases are evident in the moisture transport from AS to SCI in the B-MME models leading to the biases in precipitation. However, B-MME overestimates the moisture over

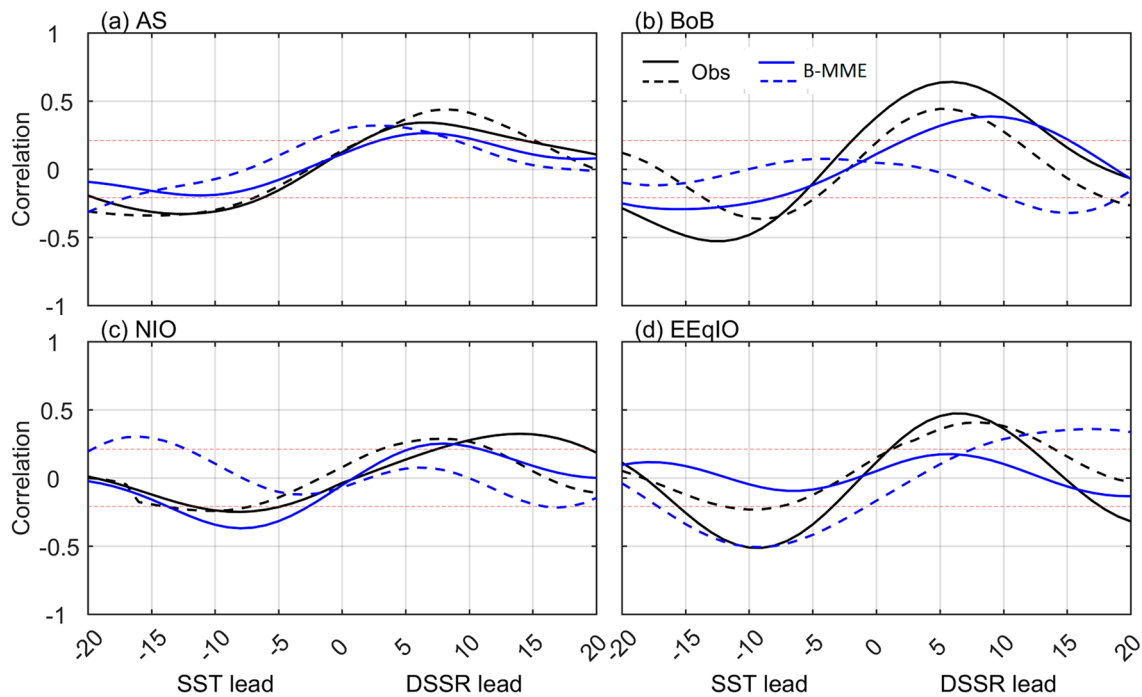


Fig. 10 Intraseasonal response (lead-lag cross-correlation) for surplus (solid) and deficit (dashed) monsoon years in the observations, B-MME models. Lead-lag cross-correlation of SST and DSSR

anomalies averaged over AS (a), BoB (b), NIO (c), EEq IO (d). Correlation values are statistically significant (red lines; 0.05 significance level using *t* test)

south peninsular India, and underestimation is evident over central India and the equatorial Indian Ocean.

ISMR exhibits strong intraseasonal and interannual variability (Goswami et al. 1999; Gadgil and Gadgil 2006; Turner and Annamalai, 2012) and is tied with the teleconnections like ENSO and IOD leading to surplus/deficit monsoonal rainfall over India (Ju and Slingo 1995). B-MME models show that wet biases of precipitation over south peninsular India are associated with the strong moisture transport from the WIO to the mainland of India. The composite of SST analysis further reveals that B-MME fails to capture the positive IOD-like patterns and overestimates the SST anomalies compared to the observations during the surplus monsoon years. The B-MME misrepresentation of SST and moisture transport mainly signifies precipitation biases over the Indian mainland during surplus and deficit monsoons. On intraseasonal timescales, convection anomalies propagate northward and eastward. The northward propagating convection anomalies phase speed is about 1.2 °lat/day. However, sluggish (fast) propagation of convection is observed in the surplus (deficit) monsoon years. The sluggish propagation of convection anomalies leads to a longer duration of convection activity and causes heavy precipitation over the region. B-MME is able to capture the northward propagation of convection anomalies with a phase speed of 0.95 °lat/day (seasonal mean). The phase speed of eastward propagating convection anomalies reveals that, during surplus (deficit)

monsoon years, convection shows the sluggish (quick) propagation to the western Pacific with a phase speed of 3.48 (4.18) °lon/day. Compared to the observations, B-MME overestimates (underestimates) the phase speed of convection during surplus (deficit) monsoons.

Further, the simulation of air-sea interactions by the B-MME and individual models on intraseasonal timescales are analysed over AS, BoB, SCI, NIO, and EEq IO regions. The response from the ocean to the atmosphere is quick (slow) over AS (BoB) on intraseasonal timescales, even though basins are located on the same latitudes. However, models represent the slow response from the ocean to the atmosphere over AS. During surplus (deficit) monsoon years, the ocean response to the atmosphere is weak (strong) is associated with the stronger SST gradients and cloud cover over the regions. Over BoB, the response is strong during surplus monsoon years than the deficit monsoon years, is associated with the large influx of freshwater to the BoB in the surplus monsoon years, and leads to basin-wide warming. The underlying SST anomalies modulate the ocean’s response to the atmosphere during surplus/deficit monsoon years, further influencing the phase speed of the precipitation anomalies. The models well simulated the ocean to atmosphere response but failed to represent the atmosphere to ocean response. B-MME fails to capture the in-phase relationship of U850 with SST and precipitation, leads to the significant underestimation/overestimation of

low-level winds and SST. Models (except CNRM-ESM2-1) well simulated the in-phase relationship of low-level SHUM and precipitation. It is identified that the CMIP6 GCMs have differed in simulating the ISM's prominent features because of the differences in their ability to represent air-sea interactions over the Indian region accurately. To overcome the simulation of the ISM by the GCMs, the ocean to atmosphere feedback mechanisms, sensitivities of the models among internal variables need to be improved. In addition, cold SST biases in the B-MME models can suppress the precipitation. The better simulation of SST in the GCMs may lead to accurate precipitation simulation.

Supplementary Information The online version contains supplementary material available at <https://doi.org/10.1007/s00382-022-06367-1>.

Acknowledgements Authors would like to acknowledge the Science and Engineering Research Board (SERB), Government of India (Grant Ref: ECR/2016/001896). Authors also want to acknowledge the World Climate Research programme's Working Group on Coupled Modelling, which is responsible for CMIP, and we thank the climate modelling groups for producing and making available their model output.

Funding This research is supported by the Science and Engineering Research Board (Grants Number ECR/2016/001896).

Data availability Data relevant to the paper can be downloaded from websites listed below: IMD precipitation: https://imd pune.gov.in/Clim_Pred_LRF_New/Grided_Data_Download.html. TRMM precipitation and SST: https://disc.gsfc.nasa.gov/datasets/TRMM_3B42_Daily_7. CMIP6 datasets: <https://esgf-node.llnl.gov/search/cmip6/>

Declarations

Conflict of interest Corresponding author declares on behalf of all the authors, there is no competing interest that influence the outcome reported in this manuscript.

References

- Ahn MS, Kim D, Kang D, Lee J, Sperber KR, Gleckler PJ, Jiang X, Ham YG, Kim H (2020) MJO propagation across the maritime continent: are CMIP6 models better than CMIP5 models? *Geophys Res Lett* 47(11):p.e2020GL087250. <https://doi.org/10.1029/2020GL087250>
- Almazroui M, Saeed F, Saeed S et al (2020) Projections of precipitation and temperature over the South Asian countries in CMIP6. *Earth Syst Environ* 4:297–320. <https://doi.org/10.1007/s41748-020-00157-7>
- Almazroui M, Saeed F, Saeed S et al (2021) Projected changes in climate extremes using CMIP6 simulations over SREX regions. *Earth Syst Environ* 5:481–497. <https://doi.org/10.1007/s41748-021-00250-5>
- Anandh PC, Vissa NK (2020) On the linkage between extreme rainfall and the Madden-Julian Oscillation over the Indian region. *Meteorol Appl* 27(2):e1901. <https://doi.org/10.1002/met.1901>
- Annamalai H, Slingo JM (2001) Active/break cycles: diagnosis of the intraseasonal variability of the Asian summer monsoon. *Clim Dyn* 18(1):85–102. <https://doi.org/10.1007/s003820100161>
- Annamalai H, Hamilton K, Sperber KR (2007) The South Asian summer monsoon and its relationship with ENSO in the IPCC AR4 simulations. *J Clim* 20(6):1071–1092
- Ashok K, Guan Z, Yamagata T (2001) Impact of the Indian Ocean dipole on the relationship between the Indian monsoon rainfall and ENSO. *Geophys Res Lett* 28(23):4499–4502. <https://doi.org/10.1029/2001GL013294>
- Ashok K, Guan Z, Saji NH, Yamagata T (2004) Individual and combined influences of ENSO and the Indian Ocean dipole on the Indian summer monsoon. *J Clim* 17(16):3141–3155.
- Ashok K, Behera SK, Rao SA, Weng H, Yamagata T (2007) El Niño Modoki and its possible teleconnection. *J Geophys Res Oceans*. <https://doi.org/10.1029/2006JC003798>
- Ashok K, Feba F, Tejavath CT (2019) The Indian summer monsoon rainfall and ENSO. *Mausam* 70(3):443–452
- Bracco A, Kucharski F, Molteni F, Hazeleger W, Severijns C (2007) A recipe for simulating the interannual variability of the Asian summer monsoon and its relation with ENSO. *Clim Dyn* 28(5):441–460
- Chakravorty S, Gnanaseelan C, Pillai PA (2016) Combined influence of remote and local SST forcing on Indian Summer Monsoon Rainfall variability. *Clim Dyn* 47(9):2817–2831
- Cherchi A, Navarra A (2013) Influence of ENSO and of the Indian Ocean Dipole on the Indian summer monsoon variability. *Clim Dyn* 41(1):81–103
- Chowdary JS, Bandgar A, Gnanaseelan C, Jing-Jia L (2015) Role of tropical Indian Ocean air–sea interactions in modulating Indian summer monsoon in a coupled mode. *Atm Sci Let* 16:170–176
- Chowdary JS, Parekh A, Kakatkar R, Gnanaseelan C, Srinivas G, Singh P, Roxy MK (2016) Tropical Indian Ocean response to the decay phase of El Niño in a coupled model and associated changes in south and east-Asian summer monsoon circulation and rainfall. *Clim Dyn* 47(3):831–844. <https://doi.org/10.1007/s00382-015-2874-9>
- Chowdary JS, Patekar D, Srinivas G, Gnanaseelan C, Parekh A (2019) Impact of the Indo-Western Pacific Ocean capacitor mode on South Asian summer monsoon rainfall. *Clim Dyn* 53:2327
- Dai X, Yang Y, Wang P (2022) Asian monsoon projection with a new large-scale monsoon definition. *Theoret Appl Climatol* 147(3):1003–1013
- Dandi RA, Chowdary JS, Pillai PA, Sidhan NSS, SSVS R, (2020) Impact of El Niño Modoki on Indian summer monsoon rainfall: Role of western north Pacific circulation in observations and CMIP5 models. *Int J Climatol* 40(4):2117–2133
- Dee DP, Uppala SM, Simmons AJ, Berrisford P, Poli P, Kobayashi S, Andrae U, Balsameda MA, Balsamo G, Bauer DP, Bechtold P (2011) The ERA-Interim reanalysis: configuration and performance of the data assimilation system. *Q J R Meteorol Soc* 137(656):553–597. <https://doi.org/10.1002/qj.828>
- DeMott CA, Stan C, Randall DA (2013) Northward propagation mechanisms of the boreal summer intraseasonal oscillation in the ERA-Interim and SP-CCSM. *J Clim* 26(6):1973–1992
- DeMott CA, Klingaman NP, Woolnough SJ (2015) Atmosphere-ocean coupled processes in the Madden-Julian oscillation. *Rev Geophys* 53(4):1099–1154. <https://doi.org/10.1002/2014RG000478>
- DeMott CA, Benedict JJ, Klingaman NP, Woolnough SJ, Randall DA (2016) Diagnosing ocean feedbacks to the MJO: SST-modulated surface fluxes and the moist static energy budget. *J Geophys Res Atmos* 121(14):8350–8373
- Duchon CE (1979) Lanczos filtering in one and two dimensions. *J Appl Meteorol Climatol* 18(80):1016–1022
- Dutta U, Chaudhari HS, Hazra A, Pokhrel S, Saha SK, Veeranjaneyulu C (2020) Role of convective and microphysical processes on

- the simulation of monsoon intraseasonal oscillation. *Clim Dyn* 55(9):2377–2403. <https://doi.org/10.1007/s00382-020-05387-z>
- Eyring V, Bony S, Meehl GA, Senior CA, Stevens B, Stouffer RJ, Taylor KE (2016) Overview of the coupled model intercomparison project phase 6 (CMIP6) experimental design and organization. *Geosci Model Dev* 9(5):1937–1958. <https://doi.org/10.5194/gmd-9-1937-2016>
- Fu X, Wang B, Li T (2002) Impacts of air–sea coupling on the simulation of mean Asian summer monsoon in the ECHAM4 model. *Mon Weather Rev* 130(12):2889–2904. [https://doi.org/10.1175/1520-0493\(2002\)130<2889:IOASCO>2.0.CO;2](https://doi.org/10.1175/1520-0493(2002)130<2889:IOASCO>2.0.CO;2)
- Gadgil S (2003) The Indian monsoon and its variability. *Annu Rev Earth Planet Sci* 31(1):429–467
- Gadgil S, Gadgil S (2006) The Indian monsoon, GDP and agriculture. *Econ Political Wkly* 4887–4895
- Gadgil S, Vinayachandran PN, Francis PA (2004) Extremes of the Indian summer monsoon rainfall, ENSO and equatorial Indian Ocean oscillation. *Geophys Res Lett* 31:L12213
- Gao Y, Klingaman NP, DeMott CA, Hsu PC (2019) Diagnosing ocean feedbacks to the BSISO: SST-modulated surface fluxes and the moist static energy budget. *J Geophys Res Atmos* 124(1):146–170. <https://doi.org/10.1029/2018JD029303>
- Goswami BN (1998) Inter-annual variation of Indian summer monsoon in a GCM: external conditions versus internal feedbacks. *J Climatol* 11:501–522
- Goswami BN (2005) South asian monsoon. Intraseasonal variability in the atmosphere-ocean climate system. Springer, Heidelberg, pp 19–61. https://doi.org/10.1007/3-540-27250-X_2
- Goswami BN, Mohan RA (2001) Intraseasonal oscillations and interannual variability of the Indian summer monsoon. *J Clim* 14(6):1180–1198. [https://doi.org/10.1175/1520-0442\(2001\)014%3c1180:IOAIVO%3e2.0.CO;2](https://doi.org/10.1175/1520-0442(2001)014%3c1180:IOAIVO%3e2.0.CO;2)
- Goswami BN, Krishnamurthy V, Annamalai H (1999) A broad-scale circulation index for the interannual variability of the Indian summer monsoon. *Q J R Meteorol Soc* 125(554):611–633. <https://doi.org/10.1002/qj.49712555412>
- Goswami BN, Wu G, Yasunari T (2006) The annual cycle, intraseasonal oscillations, and roadblock to seasonal predictability of the Asian summer monsoon. *J Clim* 19(20):5078–5099. <https://doi.org/10.1175/JCLI3901.1>
- Goswami BB, Deshpande M, Mukhopadhyay P, Saha SK, Rao SA, Murthugudde R, Goswami BN (2014) Simulation of monsoon intraseasonal variability in NCEP CFSv2 and its role on systematic bias. *Clim Dyn* 43(9–10):2725–2745
- Goswami BB, Krishna RPM, Mukhopadhyay P, Khairoutdinov M, Goswami BN (2015) Simulation of the Indian summer monsoon in the superparameterized climate forecast system version 2: preliminary results. *J Clim* 28(22):8988–9012. <https://doi.org/10.1175/JCLI-D-14-00607.1>
- Goswami BN, Rao SA, Sengupta D, Chakravorty S (2016) Monsoons to mixing in the Bay of Bengal: multiscale air-sea interactions and monsoon predictability. *Oceanography* 29(2):18–27
- Gusain A, Ghosh S, Karmakar S (2020) Added value of CMIP6 over CMIP5 models in simulating Indian summer monsoon rainfall. *Atmosph Res* 232:104680. <https://doi.org/10.1016/j.atmosres.2019.104680>
- Hendon H (2005) Air-sea interaction. Intraseasonal variability in the atmosphere-ocean climate system. Springer, Berlin, pp 223–246
- Hrudya PH, Varikoden H, Vishnu R, Kuttippurath J (2020) Changes in ENSO-monsoon relations from early to recent decades during onset, peak and withdrawal phases of Indian summer monsoon. *Clim Dyn* 55(5):1457–1471
- Hrudya PH, Varikoden H, Vishnu R (2021) A review on the Indian summer monsoon rainfall, variability and its association with ENSO and IOD. *Meteorol Atmos Phys* 133(1):1–14
- Hsu PC, Lee JY, Ha KJ, Tsou CH (2017) Influences of boreal summer intraseasonal oscillation on heat waves in monsoon Asia. *J Clim* 30(18):7191–7211. <https://doi.org/10.1175/JCLI-D-16-0505.1>
- Huang F, Xu Z, Guo W (2020) The linkage between CMIP5 climate models' abilities to simulate precipitation and vector winds. *Clim Dyn* 54(11):4953–4970
- Huffman GJ, Adler RF, Bolvin DT, Nelkin EJ (2010) The TRMM multi-satellite precipitation analysis (TMPA). Satellite rainfall applications for surface hydrology. Springer, Dordrecht, pp 3–22. https://doi.org/10.1007/978-90-481-2915-7_1
- Jain S, Mishra SK, Anand A, Salunke P, Fasullo JT (2021) Historical and projected low-frequency variability in the Somali Jet and Indian Summer Monsoon. *Clim Dyn* 56(3):749–765. <https://doi.org/10.1007/s00382-020-05492-z>
- Jiang X, Li T, Wang B (2004) Structures and mechanisms of the northward propagating boreal summer intraseasonal oscillation. *J Clim* 17(5):1022–1039. [https://doi.org/10.1175/1520-0442\(2004\)017%3c1022:SAMOTN%3e2.0.CO;2](https://doi.org/10.1175/1520-0442(2004)017%3c1022:SAMOTN%3e2.0.CO;2)
- Joseph S, Sahai AK, Goswami BN (2009) Eastward propagating MJO during boreal summer and Indian monsoon droughts. *Clim Dyn* 32(7):1139–1153
- Joseph S, Sahai AK, Goswami BN (2010) Boreal summer intraseasonal oscillations and seasonal Indian monsoon prediction in DEMETER coupled models. *Clim Dyn* 35(4):651–667. <https://doi.org/10.1007/s00382-009-0635-3.pdf>
- Ju J, Slingo J (1995) The Asian summer monsoon and ENSO. *Q J R Meteorol Soc* 121(525):1133–1168
- Karmakar N, Misra V (2019) The relation of intraseasonal variations with local onset and demise of the Indian summer monsoon. *J Geophys Res Atmos* 124(5):2483–2506
- Karmakar N, Misra V (2020) Differences in northward propagation of convection over the Arabian Sea and Bay of Bengal during boreal summer. *J Geophys Res Atmos*. <https://doi.org/10.1029/2019JD031648>
- Karmakar N, Boos WR, Misra V (2021) Influence of intraseasonal variability on the development of monsoon depressions. *Geophys Res Lett* 48(2):p.e2020GL090425
- Kikuchi K, Wang B, Kajikawa Y (2012) Bimodal representation of the tropical intraseasonal oscillation. *Clim Dyn* 38(9):1989–2000. <https://doi.org/10.1007/s00382-011-1159-1>
- Konda G, Vissa NK (2019) Intraseasonal convection and air–sea fluxes over the Indian monsoon region revealed from the Bimodal ISO index. *Pure Appl Geophys* 176(8):3665–3680. <https://doi.org/10.1007/s00024-019-02119-1>
- Konda G, Vissa NK (2021) Assessment of ocean-atmosphere interactions for the boreal summer intraseasonal oscillations in CMIP5 models over the Indian monsoon region. *Asia-Pacific J Atmos Sci*. <https://doi.org/10.1007/s13143-021-00228-3>
- Kripalani RH, Kulkarni A (1997) Climatological impact of El Niño /La Niña on the Indian monsoon: a new perspective. *Weather* 52:39–46
- Kripalani RH, Oh JH, Kulkarni A, Sabade SS, Chaudhari HS (2007) South Asian summer monsoon precipitation variability: coupled climate model simulations and projections under IPCC AR4. *Theoret Appl Climatol* 90(3):133–159
- Krishnamurthy V, Ajayamohan RS (2010) Composite structure of monsoon low pressure systems and its relation to Indian rainfall. *J Clim* 23(16):4285–4305
- Krishnamurthy V, Goswami BN (2000) Indian monsoon-ENSO relationship on interdecadal timescale. *J Clim* 13(3):579–595. [https://doi.org/10.1175/1520-0442\(2000\)013%3C0579:IMEROI%3E2.0.CO;2](https://doi.org/10.1175/1520-0442(2000)013%3C0579:IMEROI%3E2.0.CO;2)
- Krishnamurthy V, Sharma AS (2017) Predictability at intraseasonal time scale. *Geophys Res Lett* 44(16):8530–8537. <https://doi.org/10.1002/2017GL074984>

- Krishnamurthy V, Shukla J (2007) Intraseasonal and seasonally persisting patterns of Indian monsoon rainfall. *J Clim* 20(1):3–20. <https://doi.org/10.1175/JCLI3981.1>
- Krishnan R, Ramesh KV, Samala BK, Meyers G, Slingo JM, Fennesy MJ (2006) Indian Ocean-monsoon coupled interactions and impending monsoon droughts. *Geophys Res Lett.* <https://doi.org/10.1029/2006GL025811>
- Krishnan R, Kumar V, Sugi M, Yoshimura J (2009) Internal feedbacks from monsoon–midlatitude interactions during droughts in the Indian summer monsoon. *J Atmos Sci* 66(3):553–578
- Krishnan R, Sundaram S, Swapna P, Kumar V, Ayantika DC, Mujumdar M (2011) The crucial role of ocean–atmosphere coupling on the Indian monsoon anomalous response during dipole events. *Clim Dyn* 37(1–2):1–17
- Krishnaswamy J, Vaidyanathan S, Rajagopalan B, Bonell M, Sankaran M, Bhalla RS, Badiger S (2015) Non-stationary and non-linear influence of ENSO and Indian Ocean Dipole on the variability of Indian monsoon rainfall and extreme rain events. *Clim Dyn* 45(1–2):175–184
- Kucharski F, Abid MA., 2017. Interannual variability of the Indian monsoon and its link to ENSO. In *Oxford Research Encyclopedia of Climate Science*.
- Kulkarni A, Sabade SS, Kripalani RH (2009) Spatial variability of intra-seasonal oscillations during extreme Indian monsoons. *Int J Climatol* 29(13):1945–1955
- Kulkarni MA, Acharya N, Kar SC, Mohanty UC, Tippett MK, Robertson AW, Luo JJ, Yamagata T (2012) Probabilistic prediction of Indian summer monsoon rainfall using global climate models. *Theoret Appl Climatol* 107(3):441–450. <https://doi.org/10.1007/s00704-011-0493-x>
- Kumar KK, Rajagopalan B, Cane MA (1999) On the weakening relationship between the Indian Monsoon and ENSO. *Science* 284(5423):2156–2159
- Kumar OB, Rao SR, Ranganathan S, Raju SS (2010) Role of intra-seasonal oscillations on monsoon floods and droughts over India. *Asia-Pac J Atmos Sci* 46(1):21–28. <https://doi.org/10.1007/s13143-010-0003-6.pdf>
- Lawrence DM, Webster PJ (2001) Interannual variations of the intra-seasonal oscillation in the South Asian summer monsoon region. *J Clim* 14(13):2910–2922
- Lawrence DM, Webster PJ (2002) The boreal summer intraseasonal oscillation: relationship between northward and eastward movement of convection. *J Atmos Sci* 59(9):1593–1606. [https://doi.org/10.1175/1520-0469\(2002\)059%3c1593:TBSIOR%3e2.0.CO;2](https://doi.org/10.1175/1520-0469(2002)059%3c1593:TBSIOR%3e2.0.CO;2)
- Lee JY, Wang B, Wheeler MC, Fu X, Waliser DE, Kang IS (2013) Real-time multivariate indices for the boreal summer intraseasonal oscillation over the Asian summer monsoon region. *Clim Dyn* 40(1–2):493–509. <https://doi.org/10.1007/s00382-012-1544-4.pdf>
- Levine RC, Turner AG (2012) Dependence of Indian monsoon rainfall on moisture fluxes across the Arabian Sea and the impact of coupled model sea surface temperature biases. *Clim Dyn* 38(11):2167–2190
- Li J, Lu X (2020) SABER observations of gravity wave responses to the Madden-Julian oscillation from the stratosphere to the lower troposphere in tropics and extratropics. *Geophys Res Lett* 47(23):014. <https://doi.org/10.1029/2020GL091014>
- Li L, Zhai P, Chen Y, Ni Y (2016) Low-frequency oscillations of the East Asia-Pacific teleconnection pattern and their impacts on persistent heavy precipitation in the Yangtze-Huai River valley. *J Meteorol Res* 30(4):459–471. <https://doi.org/10.1007/s13351-016-6024-z>
- Madden RA, Julian PR (1971) Detection of a 40–50 day oscillation in the zonal wind in the tropical Pacific. *J Atmos Sci* 28(5):702–708.
- Madden RA, Julian PR (1972) Description of global-scale circulation cells in the tropics with a 40–50 day period. *J Atmos Sci* 29(6):1109–1123. [https://doi.org/10.1175/1520-0469\(1972\)029%3c1109:DOGSCC%3e2.0.CO;2](https://doi.org/10.1175/1520-0469(1972)029%3c1109:DOGSCC%3e2.0.CO;2)
- Mahadevan A, Jaeger GS, Freilich M, Omand MM, Shroyer EL, Sengupta D (2016) Freshwater in the Bay of Bengal: its fate and role in air-sea heat exchange. *Oceanography* 29(2):72–81
- Mao J, Chan JC (2005) Intraseasonal variability of the South China Sea summer monsoon. *J Clim* 18(13):2388–2402
- Mishra AK, Singh VP (2010) A review of drought concepts. *J Hydrol* 391(1–2):202–216
- Mishra V, Smoliak BV, Lettenmaier DP, Wallace JM (2012) A prominent pattern of year-to-year variability in Indian summer monsoon rainfall. *Proc Natl Acad Sci* 109(19):7213–7217
- Neena JM, Waliser D, Jiang X (2017) Model performance metrics and process diagnostics for boreal summer intraseasonal variability. *Clim Dyn* 48(5–6):1661–1683
- Pai DS, Sridhar L, Guhathakurta P, Hatwar HR (2011) District-wide drought climatology of the southwest monsoon season over India based on standardized precipitation index (SPI). *Nat Hazards* 59(3):1797–1813. <https://doi.org/10.1007/s11069-011-9867-8.pdf>
- Pai DS, Rajeevan M, Sreejith OP, Mukhopadhyay B, Satbha NS (2014) Development of a new high spatial resolution (0.25×0.25) long period (1901–2010) daily gridded rainfall data set over India and its comparison with existing data sets over the region. *Mausam* 65(1):1–18
- Pai DS, Sridhar L, Rajeevan M, Sreejith OP, Satbhai NS, Mukhopadhyay B (2014) Development of a new high spatial resolution (0.25 × 0.25) long period (1901–2010) daily gridded rainfall data set over India and its comparison with existing data sets over the region. *Mausam* 65(1):1–8
- Pai DS, Guhathakurta P, Kulkarni A, Rajeevan MN (2017) Variability of meteorological droughts over India. Observed climate variability and change over the Indian Region. Springer, Singapore, pp 73–87. https://doi.org/10.1007/978-981-10-2531-0_5
- Pandey P, Dwivedi S, Goswami BN, Kucharski F (2020) A new perspective on ENSO-Indian summer monsoon rainfall relationship in a warming environment. *Clim Dyn* 55(11):3307–3326
- Paramita M, Sutapa C, Debanjana D, Das A (2020) Impact of vertical structure of the atmosphere on the variability in summer monsoon rainfall over Gangetic West Bengal, India. *Theor Appl Climatol* 140(3–4):1359–1371
- Pathak R, Sahany S, Mishra SK, Dash SK (2019) Precipitation biases in CMIP5 models over the south Asian region. *Sci rep* 9(1):1–13
- Patil C, Prabhakaran T, Ray KS, Karipot A (2019) Revisiting moisture transport during the Indian summer monsoon using the moisture river concept. *Pure Appl Geophys* 176(11):5107–5123
- Peng J, Dadson S, Leng G, Duan Z, Jagdhuber T, Guo W, Ludwig R (2019) The impact of the Madden-Julian Oscillation on hydrological extremes. *J Hydrol* 571:142–149
- Pillai PA, Chowdary JS (2016) Indian summer monsoon intra-seasonal oscillation associated with the developing and decaying phase of El Niño. *Int J Climatol* 36(4):1846–1862. <https://doi.org/10.1002/joc.4464>
- Power S, Casey T, Folland C, Colman A, Mehta V (1999) Interdecadal modulation of the impact of ENSO on Australia. *Clim Dyn* 15(5):319–324
- Preethi B, Mujumdar M, Kripalani RH, Prabhu A, Krishnan R (2017a) Recent trends and tele-connections among South and East Asian summer monsoons in a warming environment. *Clim Dyn* 48(7–8):2489–2505. <https://doi.org/10.1007/s00382-016-3218-0.pdf>
- Preethi B, Mujumdar M, Prabhu A, Kripalani R (2017b) Variability and teleconnections of South and East Asian summer

- monsoons in present and future projections of CMIP5 climate models. *Asia-Pac J Atmos Sci* 53(2):305–325. <https://doi.org/10.1007/s13143-017-0034-3>
- Preethi B, Ramya R, Patwardhan SK, Mujumdar M, Kripalani RH (2019) Variability of Indian summer monsoon droughts in CMIP5 climate models. *Clim Dyn* 53(3):1937–1962. <https://doi.org/10.1007/s00382-019-04752-x>
- Rajeevan M, Bhate J, Kale JD, Lal B (2006) High resolution daily gridded rainfall data for the Indian region: analysis of break and active monsoon spells. *Curr Sci* 91:296–306
- Rajeevan M, Bhate J, Jaswal AK (2008) Analysis of variability and trends of extreme rainfall events over India using 104 years of gridded daily rainfall data. *Geophys Res Lett* 35(18):18707
- Rajeevan M, Gadgil S, Bhate J (2010) Active and break spells of the Indian summer monsoon. *J Earth Syst Sci* 119(3):229–247. <https://doi.org/10.1007/s12040-010-0019-4.pdf>
- Rajendran K, Kitoh A (2006) Modulation of tropical intraseasonal oscillations by ocean–atmosphere coupling. *J Clim* 19(3):366–391
- Rajendran K, Surendran S, Varghese SJ, Sathyanath A (2021) Simulation of Indian summer monsoon rainfall, interannual variability and teleconnections: evaluation of CMIP6 models. <https://doi.org/10.1007/s00382-021-06027-w>
- Rasmusson EM, Wallace JM (1983) Meteorological aspects of the El Niño/southern oscillation. *Science* 222(4629):1195–1202. <https://doi.org/10.1126/science.222.4629.1195>
- Ratnam JV, Giorgi F, Kaginalkar A, Cozzini S (2009) Simulation of the Indian monsoon using the RegCM3–ROMS regional coupled model. *Clim Dyn* 33(1):119–139. <https://doi.org/10.1007/s00382-008-0433-3.pdf>
- Rienecker MM, Suarez MJ, Gelaro R, Todling R, Bacmeister J, Liu E, Bosilovich MG, Schubert SD, Takacs L, Kim GK, Bloom S (2011) MERRA: NASA's modern-era retrospective analysis for research and applications. *J Clim* 24(14):3624–3648. <https://doi.org/10.1175/JCLI-D-11-00015.1>
- Roxy M, Tanimoto Y (2007) Role of SST over the Indian Ocean in influencing the intraseasonal variability of the Indian summer monsoon. *J Meteorol Soc Jpn Ser II* 85(3):349–358. <https://doi.org/10.2151/jmsj.85.349>
- Roxy M, Tanimoto Y, Preethi B, Terray P, Krishnan R (2013) Intraseasonal SST-precipitation relationship and its spatial variability over the tropical summer monsoon region. *Clim Dyn* 41(1):45–61. <https://doi.org/10.1007/s00382-012-1547-1.pdf>
- Roxy MK, Dasgupta P, McPhaden MJ, Suematsu T, Zhang C, Kim D (2019) Twofold expansion of the Indo-Pacific warm pool warps the MJO life cycle. *Nature* 575(7784):647–651. <https://doi.org/10.1038/s41586-019-1764-4>
- Sabeerali CT, Ramu Dandi A, Dhakate A, Salunke K, Mahapatra S, Rao SA (2013) Simulation of boreal summer intraseasonal oscillations in the latest CMIP5 coupled GCMs. *J Geophys Res Atmos* 118(10):4401–4420. <https://doi.org/10.1002/jgrd.50403>
- Saha S, Moorthi S, Pan HL, Wu X, Wang J, Nadiga S, Tripp P, Kistler R, Woollen J, Behringer D, Liu H (2010) The NCEP climate forecast system reanalysis. *Bull Am Meteor Soc* 91(8):1015–1058
- Saha SK, Pokhrel S, Chaudhari HS, Dhakate A, Shewale S, Sabeerali CT, Salunke K, Hazra A, Mahapatra S, Rao AS (2014) Improved simulation of Indian summer monsoon in latest NCEP climate forecast system free run. *Int J Climatol* 34(5):1628–1641. <https://doi.org/10.1002/joc.3791>
- Saha SK, Hazra A, Pokhrel S, Chaudhari HS, Sujith K, Rai A, Raha-man H, Goswami BN (2019) Unraveling the mystery of Indian summer monsoon prediction: improved estimate of predictability limit. *J Geophys Res Atmos* 124(4):1962–1974. <https://doi.org/10.1029/2018JD030082>
- Saith N, Slingo J (2006) The role of the Madden–Julian Oscillation in the El Niño and Indian drought of 2002. *Int J Climatol* 26(10):1361–1378
- Saji NH, Goswami BN, Vinayachandran PN, Yamagata T (1999) A dipole mode in the tropical Indian Ocean. *Nature* 401(6751):360–363
- Seetha CJ, Varikoden H, Babu CA, Kuttippurath J (2020) Significant changes in the ENSO–monsoon relationship and associated circulation features on multidecadal timescale. *Clim Dyn* 54(3):1491–1506
- Sengupta D, Goswami BN, Senan R (2001) Coherent intraseasonal oscillations of ocean and atmosphere during the Asian summer monsoon. *Geophys Res Lett* 28(21):4127–4130. <https://doi.org/10.1029/2001GL013587>
- Sharmila S, Joseph S, Sahai AK, Abhilash S, Chattopadhyay R (2014) Future projection of Indian summer monsoon variability under climate change scenario: an assessment from CMIP5 climate models. *Global Planet Change* 124:62–78
- Shenoi SSC, Shankar D, Shetye SR (2002) Differences in heat budgets of the near-surface Arabian Sea and Bay of Bengal: implications for the summer monsoon. *J Geophys Res Oceans* 107(C6):5–1
- Shin CS, Huang B, Zhu J, Marx L, Kinter JL (2019) Improved seasonal predictive skill and enhanced predictability of the Asian summer monsoon rainfall following ENSO events in NCEP CFSv2 hindcasts. *Clim Dyn* 52(5):3079–3098. <https://doi.org/10.1007/s00382-018-4316-y>
- Shinoda T, Hendon HH, Glick J (1998) Intraseasonal variability of surface fluxes and sea surface temperature in the tropical western Pacific and Indian Oceans. *J Clim* 11(7):1685–1702
- Shrivastava S, Kar SC, Sharma AR (2017) Intraseasonal variability of summer monsoon rainfall and droughts over central India. *Pure Appl. Geophys* 174(4):1827
- Shukla RP (2014) The dominant intraseasonal mode of intraseasonal South Asian summer monsoon. *J Geophys Res Atmos* 119(2):635–651. <https://doi.org/10.1002/2013JD020335>
- Shukla RP, Huang B (2016) Interannual variability of the Indian summer monsoon associated with the air–sea feedback in the northern Indian Ocean. *Clim Dyn* 46(5–6):1977–1990. <https://doi.org/10.1007/s00382-015-2687-x.pdf>
- Shukla RP, Shin CS (2020) Distinguishing spread among ensemble members between drought and flood Indian summer monsoon years in the Past 58 Years (1958–2015) reforecasts. *Geophys Res Lett*. <https://doi.org/10.1029/2019GL086586>
- Sikka DR (1978) Some aspects of the life history, structure and movement of monsoon depressions. Monsoon dynamics. Birkhäuser, Basel, pp 1501–1529. https://doi.org/10.1007/978-3-0348-5759-8_21
- Sikka DR (1980) Some aspects of the large-scale fluctuations of summer monsoon rainfall over India in relation to fluctuations in planetary and regional scale circulation parameters. *Proc Indian Acad Sci Earth Planet Sci* 89:179–195
- Sikka DR, Ratna SB (2011) On improving the ability of a high-resolution atmospheric general circulation model for dynamical seasonal prediction of the extreme seasons of the Indian summer monsoon. *Mausam* 62(3):339–360
- Singh C, Dasgupta P (2017) Unraveling the spatio-temporal structure of the atmospheric and oceanic intra-seasonal oscillations during the contrasting monsoon seasons. *Atmos Res* 192:48–57
- Singh SV, Kripalani RH (1985) The south to north progression of rainfall anomalies across India during the summer monsoon season. *Pure Appl Geophys* 123(4):624–637
- Sobel AH, Nilsson J, Polvani LM (2001) The weak temperature gradient approximation and balanced tropical moisture waves. *J Atmos Sci* 58(23):3650–3665
- Song F, Zhou T (2014) The climatology and interannual variability of East Asian summer monsoon in CMIP5 coupled models: does

- air–sea coupling improve the simulations? *J Clim* 27(23):8761–8777. <https://doi.org/10.1175/JCLI-D-14-00396.1>
- Srivastava A, Rao SA, Rao DN, George G, Pradhan M (2017) Structure, characteristics, and simulation of monsoon low-pressure systems in CFS v2 coupled model. *J Geophys Res Oceans* 122(8):6394–6415. <https://doi.org/10.1002/2016JC012322>
- Srivastava G, Chakraborty A, Nanjundiah RS (2019) Multidecadal seesaw of the impact of ENSO on Indian and West African summer monsoon rainfall. *Clim Dyn* 52(11):6633–6649
- Straub KH, Kiladis GN (2003) Interactions between the boreal summer intraseasonal oscillation and higher-frequency tropical wave activity. *Mon Weather Rev* 131(5):945–960. [https://doi.org/10.1175/1520-0493\(2003\)131%3c0945:IBTBSI%3e2.0.CO;2](https://doi.org/10.1175/1520-0493(2003)131%3c0945:IBTBSI%3e2.0.CO;2)
- Suhas E, Neena JM, Goswami BN (2011) Interannual variability of Indian summer monsoon arising from interactions between seasonal mean and intraseasonal oscillations. *J Atmos Sci* 69(6):1761–1774. <https://doi.org/10.1175/JAS-D-11-0211.1>
- Suhas E, Neena JM, Goswami BN (2013) An Indian monsoon intraseasonal oscillations (MISO) index for real time monitoring and forecast verification. *Clim Dyn* 40(11–12):2605–2616. <https://doi.org/10.1007/s00382-012-1462-5.pdf>
- Sun Q, Miao C, Duan Q, Ashouri H, Sorooshian S, Hsu KL (2018) A review of global precipitation data sets: data sources, estimation, and intercomparisons. *Rev Geophys* 56(1):79–107. <https://doi.org/10.1002/2017RG000574>
- Surendran S, Gadgil S, Francis PA, Rajeevan M (2015) Prediction of Indian rainfall during the summer monsoon season on the basis of links with equatorial Pacific and Indian Ocean climate indices. *Environ Res Lett* 10(9):094004
- Swann AL, Hoffman FM, Koven CD, Randerson JT (2016) Plant responses to increasing CO2 reduce estimates of climate impacts on drought severity. *Proc Natl Acad Sci* 113(36):10019–10024. <https://doi.org/10.1073/pnas.1604581113>
- Swapna P, RameshKumar MR (2002) Role of low level flow on the summer monsoon rainfall over the Indian subcontinent during two contrasting monsoon years. *J Ind Geophys Union* 6(3):123–137
- Taylor KE (2001) Summarizing multiple aspects of model performance in a single diagram. *J Geophys Res Atmos* 106(D7):7183–7192
- Thadathil P, Gopalakrishna VV, Muraliedharan PM, Reddy GV, Araligidat N, Shenoy S (2002) Surface layer temperature inversion in the Bay of Bengal. *Deep Sea Res Part I* 49(10):1801–1818
- Turner AG, Annamalai H (2012) Climate change and the South Asian summer monsoon. *Nat Clim Chang* 2(8):587–595
- Varikoden H, Preethi B (2013) Wet and dry years of Indian summer monsoon and its relation with Indo-Pacific Sea surface temperatures. *Int J Climatol* 33(7):1761–1771
- Waliser DE (2006) Intraseasonal variability. *The Asian monsoon*. Springer, Heidelberg, pp 203–257
- Waliser DE, Jin K, Kang IS, Stern WF, Schubert SD, Wu MLC, Lau KM, Lee MI, Krishnamurthy V, Kitoh A, Meehl GA (2003) AGCM simulations of intraseasonal variability associated with the Asian summer monsoon. *Clim Dyn* 21(5):423–446. <https://doi.org/10.1007/s00382-003-0337-1>
- Wang B (2005) Theory. *Intraseasonal variability in the atmosphere-ocean climate system*. Springer, Heidelberg, pp 307–360
- Wang B (2006) *The Asian monsoon*. Springer, Heidelberg
- Wang B, Li T (2004) East Asian monsoon-ENSO interactions. *East Asian monsoon*. World Scientific, London, pp 177–212. https://doi.org/10.1142/9789812701411_0005
- Wang S, Sobel AH, Tippett MK, Vitart F (2019) Prediction and predictability of tropical intraseasonal convection: seasonal dependence and the Maritime Continent prediction barrier. *Clim Dyn* 52(9):6015–6031
- Webster PJ, Magana VO, Palmer TN, Shukla J, Tomas RA, Yanai MU, Yasunari T (1998) Monsoons: processes, predictability, and the prospects for prediction. *J Geophys Res Oceans* 103(C7):14451–14510. <https://doi.org/10.1029/97JC02719>
- Xin X, Wu T, Zhang J, Yao J, Fang Y (2020) Comparison of CMIP6 and CMIP5 simulations of precipitation in China and the East Asian summer monsoon. *Int J Climatol* 40(15):6423–6440. <https://doi.org/10.1002/joc.6590>
- Yadav RK (2017) On the relationship between east equatorial Atlantic SST and ISM through Eurasian wave. *Clim Dyn* 48(1–2):281–295
- Yadav RK, Srinivas G, Chowdary JS (2018a) Atlantic Niño modulation of the Indian summer monsoon through Asian jet. *NPJ Clim Atmos Sci* 1(1):1–11
- Yadav RK, Srinivas G, Chowdary JS (2018b) Atlantic Niño modulation of Indian summer monsoon through Asian Jet. *NPJ Clim Atmos Sci* 1:1–23
- Yamaura T, Kajikawa Y (2017) Decadal change in the boreal summer intraseasonal oscillation. *Clim Dyn* 48(9–10):3003–3014
- Yang X, Huang P (2021) Restored relationship between ENSO and Indian summer monsoon rainfall around 1999/2000. *Innovation* 2(2):100102
- Yang B, Zhang Y, Qian Y, Song F, Leung LR, Wu P, Guo Z, Lu Y, Huang A (2019) Better monsoon precipitation in coupled climate models due to bias compensation. *NPJ Clim Atmos Sci* 2(1):1–8. <https://doi.org/10.1038/s41612-019-0100-x>
- Yun KS, Timmermann A (2018) Decadal monsoon-ENSO relationships reexamined. *Geophys Res Lett* 45(4):2014–2021. <https://doi.org/10.1002/2017GL076912>
- Zhao T, Dai A (2017) Uncertainties in historical changes and future projections of drought. Part II: model-simulated historical and future drought changes. *Clim Change* 144(3):535–548. <https://doi.org/10.1007/s10584-016-1742-x>
- Zheng B, Huang Y (2019) Mechanisms of northward-propagating intraseasonal oscillation over the South China Sea during the pre-monsoon period. *J Clim* 32(11):3297–3311. <https://doi.org/10.1175/JCLI-D-18-0391.1>
- Zhou W, Chan JC (2005) Intraseasonal oscillations and the South China Sea summer monsoon onset. *Int J Climatol* 25(12):1585–1609. <https://doi.org/10.1002/joc.1209>
- Zhou L, Murtugudde R (2014) Impact of northward-propagating intraseasonal variability on the onset of Indian summer monsoon. *J Clim* 27(1):126–139. <https://doi.org/10.1175/JCLI-D-13-00214.1>
- Zhou W, Xie SP (2017) Intermodel spread of the double-ITCZ bias in coupled GCMs tied to land surface temperature in AMIP GCMs. *Geophys Res Lett* 44(15):7975–7984. <https://doi.org/10.1002/2017GL074377>

Publisher's Note Springer Nature remains neutral with regard to jurisdictional claims in published maps and institutional affiliations.